Assessing representativity of NH_3 measurements influenced by boundary-layer dynamics and turbulent dispersion of a nearby emission source

Ruben B. Schulte[1], Margreet C. van Zanten[1,2], Bart J.H. van Stratum[1], and Jordi Vilà-Guerau de Arellano[1]

[1]Wageningen University & Research, P.O. Box 47, 6700, AA Wageningen, the Netherlands
[2]National Institute for Public Health and the Environment (RIVM), Antonie van Leeuwenhoeklaan 9, 3721, MA Bilthoven, the Netherlands

Correspondence: Ruben Schulte (ruben.schulte@wur.nl)

Abstract.

This study presents a ~~fine scale~~ fine-scale simulation approach to assess the representativity of ammonia (NH_3) measurements in proximity of an emission source. Close proximity to emission sources (< 5 km) can introduce a bias in regionally representative measurements of the NH_3 molar fraction and flux. Measurement sites should therefore be located a significant distance from emission sources, but such requirements are poorly defined and can be difficult to meet in densely agricultural regions. This study presents a consistent ~~criterium~~ criterion to assess the regional representativity of NH_3 measurements in proximity of an emission source, calculating variables that quantify the NH_3 plume dispersion using a series of numerical experiments at a fine resolution (20 m). Our ~~fine scale~~ fine-scale simulation framework with explicitly resolved turbulence enables us to distinguish between the background NH_3 and the emission plume, including realistic representations of NH_3 deposition and chemical gas-aerosol transformations. We introduce the concept of blending-distance, based on the calculation of turbulent fluctuations, to systematically analyze the impact of the emission plume on simulated measurements, relative to this background NH_3. ~~This sensitivity analysis includes systematic experiments~~ We perform a suite of systematic numerical experiments for flat homogeneous grassland, centered around the CESAR Observatory at Cabauw, to analyze the sensitivity of the blending-distance, varying meteorological factors, emission/deposition and NH_3 dependences. Considering these sensitivities, we find that NH_3 measurements at this measurement site should be located at a minimum distance of 0.5 - ~~2.5 km and 1~~ 3.0 km and 0.75 - ~~3.5~~ 4.5 km from an emission source, for NH_3 molar fraction and flux measurements, respectively. The simulation framework presented here can easily be adapted to local conditions and paves the way for future ammonia research to integrate simulations at high spatio-temporal resolution with observations of NH_3 concentrations and fluxes.

1 Introduction

Excess atmospheric nitrogen leads to an increased public health risk, through the formation of particulate matter, and causes environmental damage, as nitrogen deposition leads to eutrophication, ecosystem acidification and shifts in climate change

(Erisman and Schaap, 2004; Sutton et al., 2008; Behera et al., 2013; Erisman et al., 2013; Smit and Heederik, 2017). There can be serious societal consequences when nitrogen deposition critical loads are exceeded, as is the case in the Netherlands where the nitrogen crisis threatens the Dutch environment and economy (Stokstad, 2019). Atmospheric ammonia (NH_3) plays a key role in this process, mainly originating from agricultural activities and accounting for two-thirds of all nitrogen deposition in the Netherlands between 2005 and 2016 (Wichink Kruit and van Pul, 2018).

It is therefore important to have a network of NH_3 concentration and deposition measurements, used for model validation and (trend) monitoring (Wichink Kruit et al., 2021). For these purposes, the measurement sites in such a network must be representative for a larger region. One requirement for such regional measurement sites is to be located at sufficient distance from local NH_3 sources, as local emissions introduce a bias in the observations (EMEP/CCC, 2001; Wichink Kruit et al., 2021). Positioning measurements sites at sufficient distance from local sources is a challenge in densely agricultural areas like the Netherlands and regions all across the world with intensive livestock farming, e.g. North-West Germany, the province of Lerida in Spain, the state of North-Carolina in the USA or the Hai River Basin in China.

The emitted NH_3 is transported and mixed within the convective boundary layer (CBL) through turbulent dispersion. The field of turbulent plume dispersion is extensively researched using both observations and turbulent resolved models. However, such studies typically focus on concentration peaks of highly toxic/flamable gasses (Mylne and Mason, 1991; Ardeshiri et al., 2021; Cassiani et al., 2020), quantification of the emission strength and position (Shah et al., 2020; Ražnjević et al., 2021) or on statistical descriptions of the emission plume (Barad, 1958; Dosio et al., 2003; Vrieling and Nieuwstadt, 2003; Dosio and Vilà-Guerau de Arellano, 2006), typically used in chemistry transport models, e.g. OPS (Sauter et al., 2018), LOTOS-EUROS (Schaap et al., 2008) or EMEP MSC-W (Simpson et al., 2012). These transport models typically operate with resolutions at kilometer scale (1 - 50 km) and parameterized turbulence, making them unsuitable to study the impact of local NH_3 sources on nearby measurement sites at the subkilometer scale.

Furthermore, plume dispersion studies generally focus on chemically inert gasses, e.g. methane (Shah et al., 2020; Ražnjević et al., 2021). Ammonia is highly reactive: surface-atmosphere exchange and chemical gas-aerosols transformations play an important role in the NH_3 budget (Fowler et al., 1998; Van Oss et al., 1998; Nemitz et al., 2004; aan de Brugh et al., 2013; Behera et al., 2013; Shen et al., 2016; Schulte et al., 2021). Additionally, ammonia emissions in densely ~~agricultuural~~ agricultural areas are released and mixed into a background concentration, a result of long range transport of NH_3 (10-100 km). Yearly averaged background concentrations can vary from 1-2 μg m^{-3} (e.g in coastal regions) up to up to tens of μg m^{-3} in regions with intensive agricultural activity, which is the focus on this study (van Zanten et al., 2017).

In this study, we investigate the impact of a typical ammonia emission source on the regional representativeness of NH_3 concentration and flux measurements. The novelty of our approach is twofold:

- The use of a ~~fine scale~~ fine-scale Large-Eddy Simulation (LES) model with explicitly resolved turbulence at a very high spatio-temporal resolution (10-100 m and 10 s - 1 min).
- Inclusion of realistic representations of surface-atmosphere exchange, chemical gas-aerosol transformations and a background ammonia concentration.

Following this approach, we combine ~~fine scale~~ fine-scale simulations, where turbulence is explicitly resolved, with concepts of theory on turbulent emission plume dispersion and translate this knowledge to practical applications for the measurement community. The aim is to carry out a systematic analysis on how meteorological factors, including boundary-layer dynamics, deposition, chemical transformation and model resolution influence the relationships between emission and receptor. To this end, we ~~indroduce~~ introduce and analyze the concept of a blending-distance (BD), i.e. the horizontal distance at which the emission plume can be considered well-mixed with respect to the background NH_3. With the concept of blending-distance, we aim to provide an estimate of the minimum required distance from a typical NH_3 emission source for regionally representative measurements.

2 Methodology

2.1 NH_3 turbulent dispersion in DALES

To understand the variations of the NH_3 budget due to turbulence and heterogeneous sources and sinks of ammonia, our approach is two folded: (a) explicit simulation of processes that govern turbulent dispersion and mixing of NH_3 and (b) identifying their individual contributions to the NH_3 molar fraction and surface-atmosphere exchange. For the former, we use the large-eddy simulation technique with a high resolution to solve explicitly turbulence. To this end, we conduct our numerical experiments using a modified version of the Dutch Atmospheric Large-Eddy Simulation (DALES) version 4.2 (Heus et al., 2010; Ouwersloot et al., 2017), with the original v4.2 freely available online (at http://doi.org/10.5281/zenodo.3759193). DALES explicitly resolves processes at scales ranging from hundred meters to ~~kilometres~~kilometers, using filtered Navier-Stokes equations with the Boussinesq approximation. The filter size is generally equal to the grid size of the simulations, with subfilter-scale processes being parameterized using one-and-a-half-order closure. The numerical experiments presented here are performed using a 20 m x 20 m x 5 m grid for a 10 km x 4.8 km x 3 km domain (500 x 240 x 600 grid points). Atmospheric NH_3 is added to DALES as a passive scalar in ppb, of which the spatial evolution is solved simultaneously with the thermodynamic variables. The boundary conditions for scalars and meteorological variables are periodic, unless stated otherwise.

The atmospheric ammonia budget is further governed by surface-atmosphere exchange and chemical gas-particle transformations (Schulte et al., 2021). We use a simplified, yet realistic, approach in our representation of these processes. NH_3 surface-atmosphere exchange is ~~modelled~~ modeled by a constant homogeneous deposition of 0.045 ppb m s^{-1} (about 0.032 μg m^{-2}s^{-1}), representative for the observed yearly average NH_3 dry deposition in the Netherlands (https://www.rivm.nl/stikstof/meten/drogedepositieNH3; Stolk et al., 2014).

The representation of the chemical gas-aerosol transformations follows the approach of the OPS model: applying a percentage per hour change in the molar fraction of gaseous NH_3 to the whole domain (van Jaarsveld, 2004). This simplified yet realistic representation of chemistry as a net removal process will reduce the reach of the emission plume. However, the model is unable to resolve potential non-linear effects of turbulent mixing on the chemical reaction rate within the plume. Turbulent dispersion of the emission plume is characterized by macromixing (meandering) and micromixing (in-plume mixing) (Vilà-Guerau de Arellano et al., 1990; Galmarini et al., 1995). The former is mainly carried out by large-scale turbulent eddies and is related to the average dispersion of the plume. Micromixing is carried out by turbulent eddies smaller than the plume and is related to the fluctuations of NH_3 and its chemical reactants. The reaction rate can slow down close to the emission source, as macromixing is the dominant dispersion process here and little micromixing occurs to supply chemical reactants from outside the plume. The extend at which turbulent mixing can limit the chemical reactions within the plume depends on the ratio of the turbulent time scales and the time scale of chemistry (Damköhler number) (Galmarini et al., 1995; Meeder and Nieuwstadt, 2000) . When the time scales of chemistry are similar to the turbulent time scales, as is the case for ammonia (aan de Brugh et al., 2013) , the reduction in the chemical reaction rate close the the source can be significant (Vilà-Guerau de Arellano et al., 2004).

Special attention is placed on the representation of the one NH_3 emission source in our domain, representing a dairy barn. Agricultural activity accounts for over 90% of the NH_3 emissions in the Netherlands and the European Union (Anys et al., 2020; Vonk et al., 2020; van Bruggen et al., 2021). Dairy farms account for approximately 50% of these agricultural NH_3 emissions, with approximately 15.000 farms with about 100 cows each on average in the Netherlands ~~(van der Peet et al., 2018; WUR, 2021)~~ (van der Peet et al., 2018; WUR, 2021). A typical cubicle stable for 80 cows has a yearly emission of about 800 kg NH_3 year^{-1} and requires 10 m^2 per cow (800 m^2 in total) (Remmelink et al., 2020, Table 10.19; RIVM, 2021, type A1). Contrary to the closed off and air filtered housing for pigs and chickens, a dairy barn is open and the ammonia-rich air can freely escape. Therefore, we are able to represent a typical 80 dairy cow barn as a surface emission source (Theobald et al., 2012) with an emission flux of 45 ppb m s^{-1} (about 32 μg m^{-2}s^{-1}) over an area of 800 m^2.

We identify the individual contributions of ammonia sources to the NH_3 molar fraction and surface-atmosphere exchange, with each source of NH_3 represented by a unique scalar. In this study, these sources are identified as a background molar fraction ($NH_{3,bg}$) and the NH_3 emission plume ($NH_{3,plume}$) from a surface emission source. The sum of these two unique scalars represents the total atmospheric ammonia ($NH_{3,total}$), as would be observed by in-field observations. Here, we modify DALES v4.2 to force the $NH_{3,plume}$ molar fraction to zero at both x-edges of the domain (west and east), preventing circulation of the emission plume in x-direction.

Further modifications to DALES v4.2 are made to include the remaining processes governing the variability of the atmospheric ammonia budget. The scalar surface flux (F_{total}), representing surface atmosphere exchange, is divided between a flux acting on the background scalar (F_{bg}) and another flux acting on the emission plume scalar (F_{plume}). The magnitude of these two fluxes is weighted by their respective molar fractions ($NH_{3,bg}$ and $NH_{3,plume}$) relative to the total NH_3 molar fraction, e.g. $F_{bg} = \frac{NH_{3,bg}}{NH_{3,total}} F_{total}$ for $NH_{3,bg}$.

The final modification adds an additional term to be added to the change in the scalar molar fraction ($\frac{S}{dt}$). This modified change in the scalar molar fraction reads: $\frac{dS}{dt} + \frac{R_{chem}}{3600} S$, with R_{chem} representing the gain/loss rate in % hour^{-1} and subscript S representing the scalar molar fraction, which can be substituted by either $NH_{3,plume}$ or $NH_{3,bg}$.

2.2 Numerical experiments

We simulate the meteorological conditions observed on 8 May 2008 at the Ruisdael CESAR ~~– Ruisdael~~ Observatory (https://ruisdael-observatory.nl/cesar/) at Cabauw in the Netherlands (51.971°N, 4.927°E), as described by aan de Brugh et al. (2013) and Barbaro et al. (2014, 2015). ~~This case is~~ The supersite, with a 213 m high mast, is located on flat (agricultural) grassland with an average height of 0.1 m and the surface elevation changes are at most a few meters over 20 km. 8 May 2008 is selected as it is widely studied and includes measurements of the NH_3 molar fraction. In May 2008, the intensive observational campaign IMPACT/EUCAARI was held, which included ammonia concentration measurements by a MARGA system (aan de Brugh et al., 2012; Mensah et al., 2012) and several additional meteorological variables, including vertical profiles and radiosondes (Kulmala et al., 2011). The ~~model is initialized following the conditions as described by Barbaro et al. (2014).~~ meteorology of this day is described in detail by Barbaro et al. (2014), where the experiment is called CESAR2008. Figures 2 and 3 by Barbaro et al. (2014) show vertical profiles and time series of, among other variables, potential temperature, specific humidity, surface fluxes and boundary layer height. The case can be characterized as typical clear-sky, fair-weather conditions with an absence of large-scale heat advection. The model is initialized following the conditions as described by Barbaro et al. (2014) and the initial and prescribed meteorological values of the ~~reference~~ experiment can be found in Barbaro et al. (2014) Table ~~1, where the experiment is called CESAR2008.~~ 1.

In the morning, a 1500 m residual layer leads to ~~a very rapid growth of the CBL~~ an overshooting of the boundry layer height around 10:30 CEST, up to roughly 1800 m. In the afternoon (12:30 – 17:00 CEST), CBL growth is weak and the thermodynamic conditions remain relatively constant (Barbaro et al., 2014). Therefore, we only study the turbulent dispersion in the afternoon, when the impact of boundary layer dynamics on the NH3 budget is minimal. The wind speed is moderate at 5.5 to 7 m s^{-1} in the afternoon, resulting in strong shear production near the surface and a strong momentum entrainment at the CBL top. The convective time scale (τ) in the afternoon is typical for convective fair-weather conditions, increasing from 18 to 27 minutes between 12:30 and 17:00 CEST. The Monin-Obukhov length fluctuates around approximately -50 m.

The numerical experiments are split into three phases: the meteorological spin-up phase, the buffer phase and the analysis phase. During the meteorological spin-up, 8:00 – 12:30 CEST, the ammonia surface-atmosphere exchange and chemical transformations are not active. These processes are activated at the start of the buffer phase, from 12:30 – 14:00 CEST. Entrainment is still an important factor until around 13:00 CEST, causing large fluctuations of the NH_3 molar fraction (> 4 ppb) as will be discussed in Sect. 3.1. The CBL is considered well-mixed around 13:00 CEST, but we extend the buffer phase with one more hour. We do so to minimize impact of earlier entrainment on the one-hour moving average used to calculate statistics during the analysis phase. The analysis phase therefore starts at 14:00 CEST until the collapse of the CBL around 17:00 CEST. The analysis phase is the focus of this study and when we analyze the impact of the emission plume on (simulated) point measurements of the NH_3 concentration and flux.

2.3 Quantifying the emission plume impact on NH_3 measurements

Inspired by the plume observation study by Mylne and Mason (1991), we introduce three variables to assess the presence of the emitted NH_3 plume and relevance of the plume fluctuations to nearby observations. These variables, intermittency factor (I), fluctuation intensity (fI) and NH_3 flux (F), are all defined by fluctuations in the NH_3 molar fraction. Fluctuations in the NH_3 molar fraction result from turbulent mixing of differences in NH_3, caused by local sinks and sources. NH_3 fluctuations are therefore found in the background molar fraction as a result of ammonia-poor air near the surface (deposition) and top of the CBL (entrainment). NH_3 fluctuations are further enhanced in proximity of surface heterogeneous surfaces. A strong local

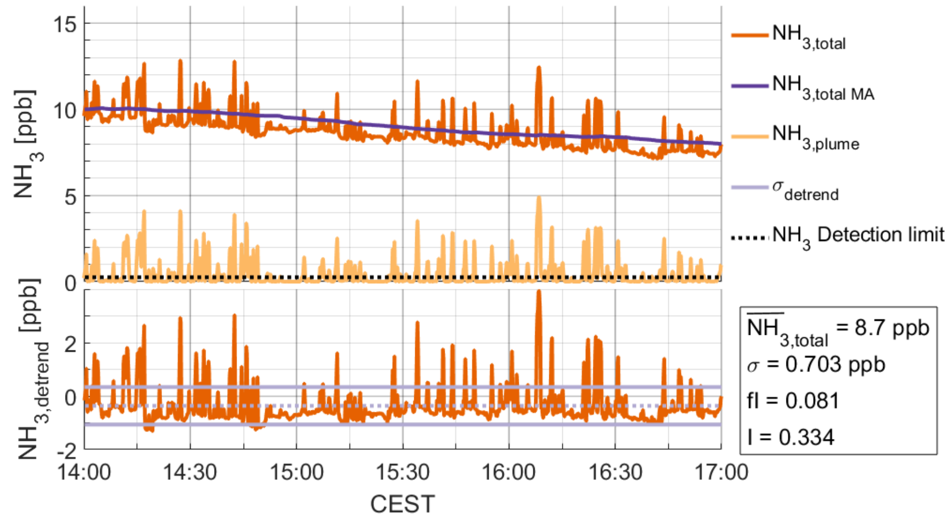

Figure 1. Top panel shows 10 s time series of $NH_{3,total}$ (orange) and $NH_{3,plume}$ (yellow) during the analysis phase, at 250 m from the emission source. The detrended $NH_{3,total}$ (orange) is shown in the bottom panel. Fluctuation intensity and intermittency are calculated following Eq. 4 and 1 respectively, based on the mean $NH_{3,total}$, standard deviation (light purple) and NH_3 detection limit (dotted black).

emission source (e.g. a dairy barn) as presented in this study, will cause an emission plume as the enhanced NH_3 molar fraction is mixed with the background molar fraction through turbulent mixing. Turbulent models like DALES explicitly resolve this turbulent mixing at high spatial-temporal resolution and can provide valuable information in the interpretation of in-field observations where surface heterogeneity plays an important role.

We first introduce the intermittency factor (I) to quantify the detectability of the emission plume. Intermittency is defined as the proportion of time during which the plume molar fraction is above the detection limit of instruments typically used to measure atmospheric ammonia, as seen in Fig. 1 and Eq. 1, where N is the number of ~~timesteps~~time steps.

$$I = \frac{1}{N}\sum_{i=1}^{N}\begin{cases}1, & \text{if } NH_{3,plume}(i) \geq 0.25ppb\\ 0, & \text{if } NH_{3,plume}(i) < 0.25ppb\end{cases} \quad (1)$$

Note that the intermittency is calculated for each individual grid point during the analysis window (14:00 - 17:00 CEST) at 10 s temporal resolution. We set the NH_3 detection limit at 0.25 ppb, similar to the detection limit of the miniDOAS instrument used in the Dutch ammonia monitoring network (Berkhout et al., 2017). The concept of intermittency cannot be applied to $NH_{3,bg}$ or $NH_{3,total}$, as the background molar fraction always exceeds 0.25 ppb in our numerical experiments, which would result in an intermittency of 1. We therefore only calculate the ~~intermittenct~~ intermittency for $NH_{3,plume}$ to analyze the detectability of the emission plume.

The second variable, fluctuation intensity (fI), determines the magnitude of the NH_3 fluctuations, i.e. NH_3 standard deviation (σ_{NH_3}), relative to the mean NH_3 molar fraction ($\overline{NH_3}$). Fluctuation intensity is defined following Eq. 2:

$$fI = \frac{\sigma_{NH_3}}{\overline{NH_3}} \quad (2)$$

The fluctuation intensity quantifies the level of turbulent mixing. High fI indicates that there are large fluctuations in the measured NH_3 which can introduce a positive bias in measurements. In the field of plume dispersion, high fI is found close to the source where plume meandering dominates the mixing process (Dosio and Vilà-Guerau de Arellano, 2006), or at the edge of the emission plume as a result of lateral entrainment of air from outside the plume (Mylne and Mason, 1991; Gailis et al., 2007; Ražnjević et al., 2021). When analyzing the fluctuation intensity of $NH_{3,total}$, we have a consistent reference for the fluctuation intensity in $NH_{3,bg}$. Comparing the fI for the total ammonia (fI_{total}) to the fI for the background ammonia (fI_{bg}), enables us to quantify the relative impact of the emitted NH_3 plume to simulated measurement. When fI_{total} is of the same order of magnitude as fI_{bg}, we consider the emission plume indistinguishable from the background NH_3, i.e. the plume is well mixed.

~~Note that~~ Note that for $NH_{3,plume}$, the average NH_3 concentration is (very close to) zero outside the emission plume, which could lead to infinitely large fluctuation intensity following Eq. 2. Therefore, fI is only calculated inside the plume, using an arbitrary requirement of $\overline{NH}_{3,plume} > 10^{-5}$ ppb.

Fig. 1 shows a downward trend in $NH_{3,bg}$ and $NH_{3,total}$, resulting from surface deposition and the loss by chemical gas-aerosol transformations. To minimize the impact of this downward trend on σ_{NH_3}, we detrend the simulated molar fraction by subtracting a 1 hour leading moving average ($NH_{3,MA}$), following Eq. 3 and shown in Fig. 1. The detrended molar fraction ($NH_{3,detrend}$) is assumed to only represent turbulent fluctuations and is used to calculate the standard deviation to derive fluctuation intensity. By using $NH_{3,detrend}$ to calculate σ_{NH_3}, the fluctuation intensity follows from Eq. 4.

$$NH_{3,detrend} = NH_3 - NH_{3,MA} \quad (3)$$

$$fI = \frac{\sigma_{NH_3}}{\overline{NH_3}} = \frac{\sqrt{\frac{1}{N-1}\sum_{i=1}^{N} |NH_{3,detrend} - (\overline{NH_{3,detrend}})|^2}}{\overline{NH_3}} \quad (4)$$

Finally, we introduce the 30 minute NH_3 flux, studied to mimic the in-field ammonia ~~eddy-covariance~~ eddy covariance flux measurements and calculated following Eq. 5. The flux presented in this study is the average 30 minute flux, for each individual grid point, over the analysis phase between 14:00 and 17:00 CEST.

$$F_{NH_3} = \overline{NH_3' w'} \quad (5)$$

2.4 The concept of blending-distance

We use the fluctuation intensity and flux to quantify the impact of the emission plume on the simulated NH_3 molar fraction and flux measurements, by introducing the concept of blending-distance. The blending-distance is based on the percentage change (PC_X) in the simulated NH_3 measurements resulting from the emission plume, i.e. the percentage change between $NH_{3,total}$ and $NH_{3,bg}$. PC_X is calculated following Eq. 6, where X can be substituted by either fI or F.

$$PC_X = \left|\frac{X_{total} - X_{bg}}{X_{bg}}\right| * 100\% \quad (6)$$

Based on this percentage change, we define a threshold for which we assume that the impact of the emission plume is negligible. The blending-distance (BD_X, is defined as the maximum distance at which PC_X drops below the threshold level (e.g. PC_X < ~~10~~25%), following Eq. 7.

$$BD_X = max(\, dist(\, PC_X < threshold \,)\,) \quad (7)$$

In this study, we present blending-distances based on an arbitrary set of threshold levels, ranging from 5% to 50%.

The concept of blending-distance is applied to the fluctuation intensity (BD_{fI}) and the NH_3 flux (BD_F) to quantify the impact on the simulated NH_3 measurements of NH_3 molar fraction and flux respectively. For context, we also present the intermittency in Sect. 3.2 to quantify the detectability of the plume.

2.5 Blending-distance sensitivity

A key aspect of the study is to determine the sensitivity of the concept of the blending-distance to variations in meteorological and NH_3 pollution factors, in order study the impact of each processes on the blending-distance and to identify the driving variables. We study the sensitivity of blending-distance for fluctuation intensity and NH_3 flux by varying the geostrophic wind speed (u_g), initial background molar fraction (C_{bg}) at the start of the analysis phase, emission strength (E), deposition strength (D), chemical conversion rate (R), simulation height (H) and model grid resolution (Δ). Table 1 presents the suite of numerical experiments presented in this study. A single numerical experiment was performed for the sensitivity studies of the NH_3 background, emission, deposition and chemistry, each with separate scalars for $NH_{3,bg}$ and $NH_{3,plume}$~~, generating~~. This single experiment, which does not include the variations in the geostrophic wind speed nor the high-resolution experiment, generates just under 1 TB of model output with a computational cost of about 64.000 SBU (System Billing Unit, i.e. the usage of one ~~core~~ processor of the Cartesius supercomputer system for one hour).

The sensitivity study is structured from large-scale processes to small scale processes and ~~modelling~~ modeling numerics. Starting with mesoscale processes, we vary the geostrophic wind speed to study the impact of the atmospheric stability on ~~blending-distrance~~blending-distance, i.e. a shear or convection dominated CBL. Atmospheric stability plays a key role in turbulent mixing of local sources (emission) and sinks (entrainment and deposition), affecting both the fluctuations in the background molar fraction and the mixing of the emission plume (Dosio et al., 2003). Next, we study the sensitivity of BD

Table 1. Parameter names, symbols, reference values and their respective variations for the sensitivity study of the blending-distance, with the reference settings highlighted in bold.

Parameters	Symobol	Reference experiment	Variations
Geostrophic wind speed	u_g	8 m s^{-1}	2 4 6 **8** 10
Initial $NH_{3\ bg}$	C_{bg}	10	5 **10** 15 25
NH_3 emission strength	E	45 ppb m s^{-1}	**45** 100 150 200
NH_3 deposition strength	D	-0.045 ppb m s^{-1}	0 -0.025 **-0.045** -0.075 -0.0100
NH_3 chemical conversion rate	R	5 % $hour^{-1}$	0 **5** 15 25
Simulated measurement height	H	37.5 m	7.5 12.5 ... 112.5 117.5
Model resolution	Δ	20 m x 20 m x 5 m	10 x 10 x 2.5 **20 x 20 x 5** 50 x 50 x 15

to different levels of the background NH_3 at the start of the analysis window, representing different levels of regional NH_3 pollution. Additionally, varying the background levels of ammonia changes the NH_3 inversion at the top of the CBL, affecting the impact of entrainment. Next, the emission strength is varied, in order to study the local effect of different emission strengths.

Furthermore, we study the sensitivity of both BD_{fI} and BD_F to NH_3 deposition and the chemical gas-aerosol transformation. These are dynamic processes, i.e. experiencing clear diurnal and seasonal variability, mainly related to temperature, humidity and pollution levels (Wichink Kruit et al., 2010; van Zanten et al., 2010; aan de Brugh et al., 2013). Our simulation approach, with a simplified representation of deposition and chemistry, allows us to distinctly study the role of these two processes.

Finally, we study the sensitivity of BD to choices made in the numerical setup of the experiments. We vary the height of the simulated measurements. The numerical experiments are generally taken at a simulated height of 37.5 m. This is a trade-off between simulating measurements close to the surface to mimic in-field observations and the resolved turbulent kinetic energy (TKE_{res}) of the model. The TKE_{res} at the lowest level of DALES (at 2.5 m) is zero due to the no-slip boundary at the surface (Heus et al., 2010). When we aim for a TKE_{res} of 75% at all three (vertical) resolutions, we find TKE_{res} of 76%, 95% and 96% for the low, middle and high resolution at 37.5 m (36.25 m for high resolution). Additionally, it is also expected that varying the measurement height will gain practical insight for in-field observations. Finally, the sensitivity of the blending-distance to changes in resolution is studied with two new numerical experiments with higher and lower resolutions of 10 m x 10 m x 2.5 m (1000 x 480 x 1200 grid points) and 50 m x 50 m x 15 m (200 x 96 x 200 grid points) respectively.

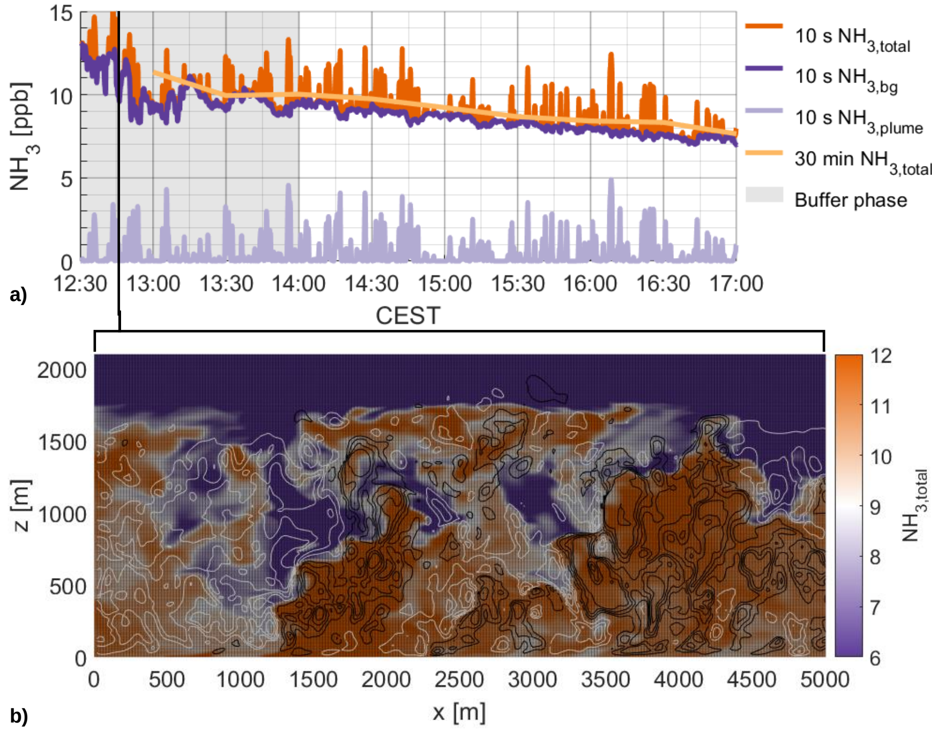

Figure 2. 10 s time series (a) of $NH_{3,total}$ (orange), $NH_{3,bg}$ (purple) and $NH_{3,plume}$ (light purple) during the buffer phase (grey area) and the analysis phase, taken at 250 m distance from the emission source. The large high-frequency fluctuations shown (> 4 ppb) are not captured by the 30 minute average of $NH_{3,total}$ (light orange). The vertical xz cross-section at 12:~~50~~ 46 CEST (b), displays high spatial variability during the buffer phase in $NH_{3,total}$ (> 4 ppb) over short distances (hundreds of meters). The black/white contour lines represent upward/downward wind speed in steps of 0.5 m s^{-1}.

3 Results

3.1 Qualitative analysis of the NH_3 emission plume impact

The concept of blending-distance is based on fluctuations in the NH_3 molar fraction. To better understand the sources of these fluctuations, we first study the time series of a "virtual" point measurement at 250 m horizontal distance from the emission source, shown in Fig. 2a. Our simulation framework allows us to ~~distinhuish~~ distinguish the individual contributions ~~to $NH_{3,total}$ (orange): NH~~of $NH_{3,bg}$ (purple) and $NH_{3,plume}$ (light purple) to $NH_{3,total}$ (orange). Here we find that the large $NH_{3,total}$ fluctuations are mainly ascribed to $NH_{3,plume}$.

As discussed in Sect. 2.3, fluctuations are also found in the background ~~concentration, $NH_{3,bg}$~~molar fraction ($NH_{3,bg}$), leading to a non-zero ~~fluctuation intensity for the background molar fraction. The high-frequency fluctuations in $NH_{3,total}$ and $NH_{3,bg}$ are filtered out when averaging over 30 minutes, the typical averaging time of in-field observations. Such turbulent fluctuations could be interpreted as noise in the raw measurement data of in-field observations.~~

The NH_3 fluctuations in NHfI_{bg}. Fluctuations $NH_{3,bg}$ are a result of heterogeneous turbulent mixingof vertical molar fraction differences in the CBL. Both . In this study, the fluctuations are caused by vertical gradients only, as we use a homogeneous surface in the simulation of $NH_{3,\,bg}$. These vertical gradients are found near the surface and at the top of the CBL, the molar fraction decreases through . At the surface, the surface-atmosphere exchange (deposition) and decreases the NH_3 molar fraction, which results in a vertical gradient in $NH_{3,bg}$. At the top of the CBL, the vertical gradient is a result of the turbulent exchange with the free troposphere (entrainment). A clear example of the impact of this turbulent mixing is shown in Fig. 2b , where the xz cross-section shows that entrainment causes a large pocket of ammonia-poor air (about 6 ppb) to reach the surface. This results in a sudden decrease of over shows that the intrusion of NH_3-low air masses from the free-troposphere are transported by the downdraft subsidence motions, resulting in large fluctuations in $NH_{3,bg}$ in the boundary layer. As shown in Fig. 2a, the amplitude of these fluctuations can reach 4 ppb in the simulated measurement, which and can last for over 5 to 15 minutes. The same process of turbulent mixing of local sinks and sources causes the fluctuations in the NH_3 molar fraction shown in Fig. 2a. minutes. When averaging over 30 minutes, even the large fluctuations between 12:30 and 13:15 are filtered out, but these high-frequency turbulent fluctuations could still be present in raw measurement data of high-resolution in-field observations.

Now that we understand the source of the NH_3 fluctuations, we take a closer look at the emission plume without any background NH_3. We only calculate fI for $NH_{3,plume}$ for $\overline{NH}_{3,plume} > 1\,10^{-5}$. The xy plot in Fig. 3a shows low fI in the plume center (≈ 2) and a strong increase near the plume edges, up to fI $\approx$ 18. 30. This is echoed by the plume transects, as they shows the typical “U-shape” found for Gaussian plumes (Mylne and Mason, 1991; Gailis et al., 2007; Ražnjević et al., 2021). These high fI values at the edges of the plume are a result of very low average molar fractions combined with low intermittency. This leads to a high standard deviation, relative to the very low averaged molar fraction, at the plume edges. Without background NH_3, it is at the edges of the plume that in-plume lateral entrainment of ammonia-free air happens, diluting the emission plume by turbulent mixing.

The intermittency cross-section in Fig. 3b shows that maximum I is only a little over 0.3, resulting from the meandering of the plume. Figure 3b also shows that, with an NH_3 detection limit of 0.25 ppb, the plume can be detected up to a distance of about 2.5 2.0 km from the source.

The cross-section of fI changes dramatically when analyzing $NH_{3,total}$, the sum of $NH_{3,bg}$ and $NH_{3,plume}$. With the addition of a non-zero background molar fraction, fI can be calculated over the whole domain, as shown in Fig. 3c. Now, we find a much lower fluctuation intensity, with a maximum of 0.08 for $NH_{3,total}$ compared to 18 30 for $NH_{3,plume}$. The U-shape in shown in the transect of Fig. 3a is replaced by an approximately Gaussian shape, with the highest fluctuation intensities at the centreline centerline of the plume. This centreline centerline fI decreases with distance from the source and becomes indistinguishable from the out-of-plume fI after approximately 1 km distance, i.e. a rough estimate for BD_{fI}.

Finally, Fig. 3d shows that the emission plume leads to a positive flux (emission) for $NH_{3,total}$ in proximity of the emission source, while the flux is negative (deposition) outside the plume. Note that significant fluctuations are found in the flux over the full domain, with $\sigma_{F,bg}$ = 0.006 0.0065 ppb m s^{-1} (prescribed $F_{sfc.}$ = -0.045 ppb m s^{-1}) for $NH_{3,bg}$. Similar to fI_{total} in Fig. 3c, the transects for the NH_3 flux are approximately gaussian in shape, with the peak values close to the plume centreline centerline at $y/y_{plume} = 0$. After approximately 1 km at the approximate plume centrelinecenterline, the in-plume flux becomes visually

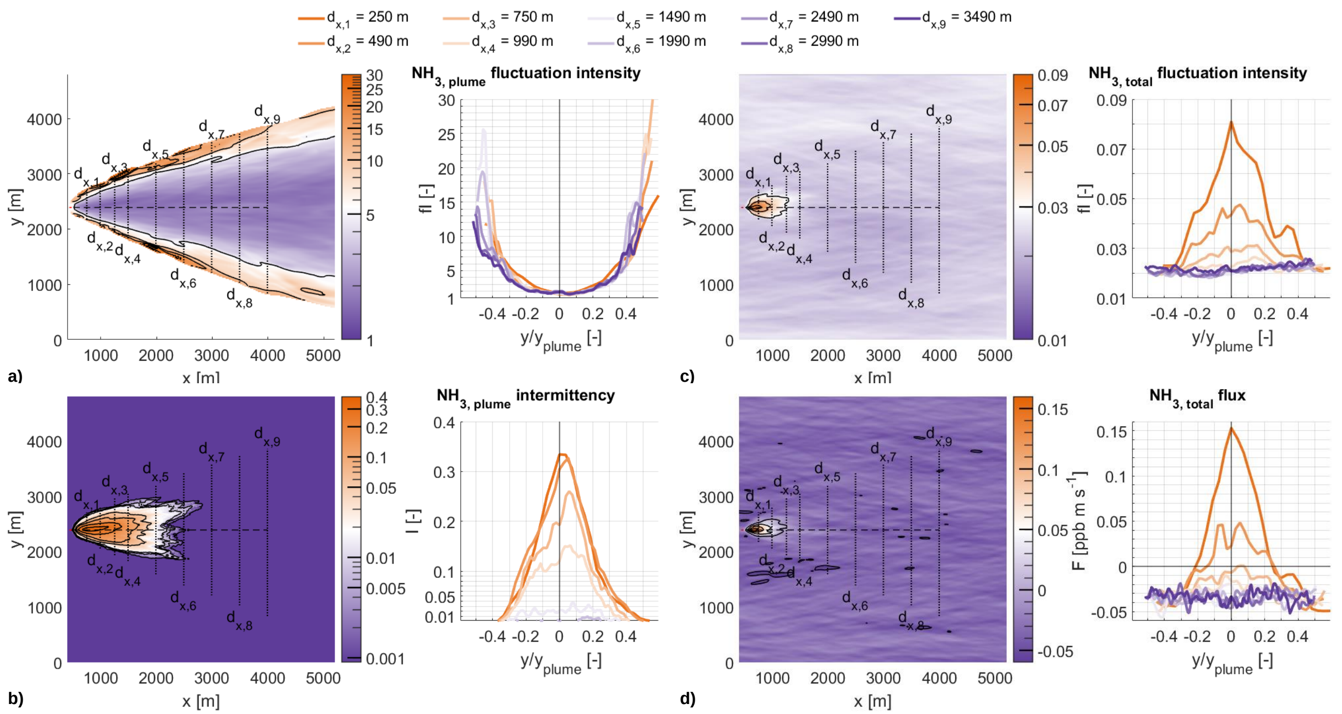

Figure 3. The xy cross-sections at 37.5 m with y-transects through the NH_3 emission plume for the $NH_{3,plume}$ fluctuation intensity (a), intermittency (b), $NH_{3,total}$ fluctuation intensity (c) and $NH_{3,total}$ flux (d). The plume transects are ~~labelend~~ labeled $d_{x,1}$ to $d_{x,9}$ for increasing x-distance from the NH_3 emission source and normalized by plume width for $NH_{3,plume} >$ ~~1~~ 10^{-5} ppb. The data presented is calculated during the analysis phase (14:00 and 17:00 CEST) at 37.5 m

.

indistinguishable from the background, i.e. a rough estimate for BD_F. This positive anomaly is the result of the emission source being within the footprint of these receptors.

3.2 Quantitative analysis of the NH_3 emission plume impact

We apply the concept of blending-distance in Fig. 4 to the ~~main variables that characterize the NH_3 evolution:~~ fluctuation intensity (a), flux (b) and intermittency (c). The markers represent the value at each individual grid point on the 37.5 m horizontal plane, the continuous orange line represents the gridpoint with the highest value within a 50 m moving window (maximum~~statistics~~), the orange dotted line represents the plume ~~centreline~~ centerline and the purple dashed and continuous lines represent the blending-distances for their respective threshold. ~~Note that both the centreline and the maximum statistics give similar results, indicating that the highest values for fI, F and I are generally found at the plume centreline, though with uncertainties.~~

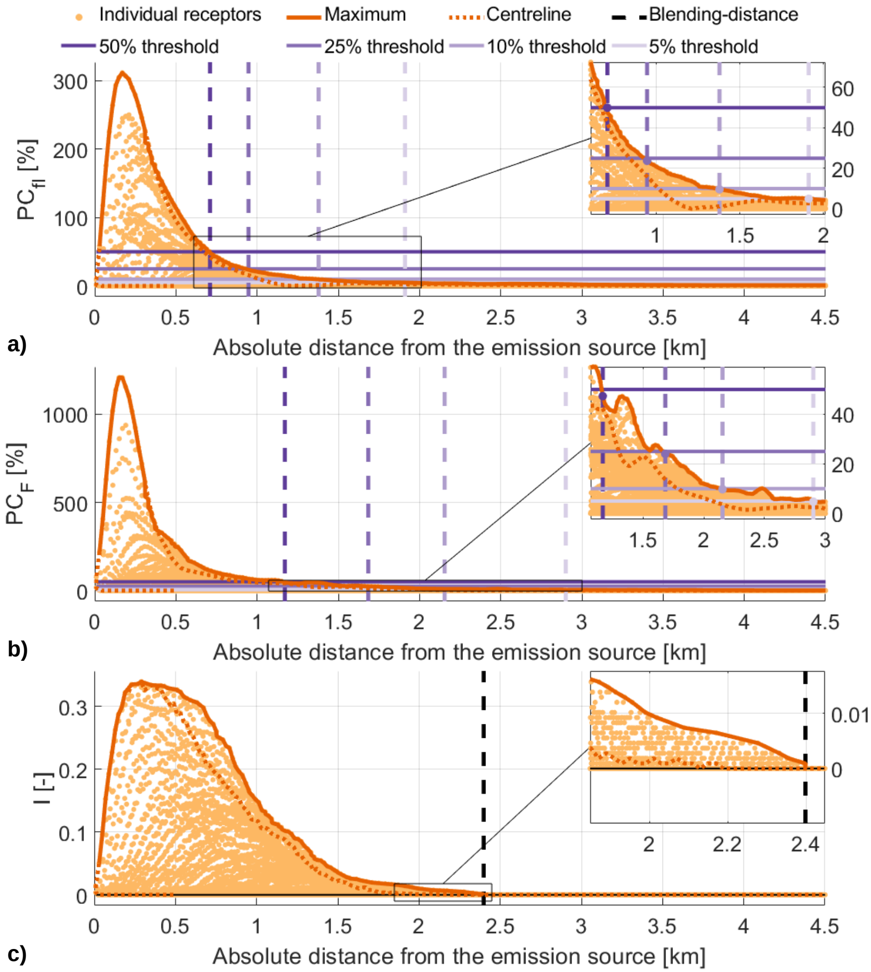

Figure 4. The percentage change of $NH_{3,total}$ relative to $NH_{3,bg}$ against absolute distance from the NH_3 emission source. The panels show fluctuation intensity (a), NH_3 flux (b) and intermittency (c). Highlighted are the maximum value within a 50 m moving window (orange) and the plume ~~centreline~~ centerline (dotted orange). Blending-distances (purple dashed) are calculated based on three thresholds at 5%, 10%~~and~~ , 25% and 50% (purple continuous).

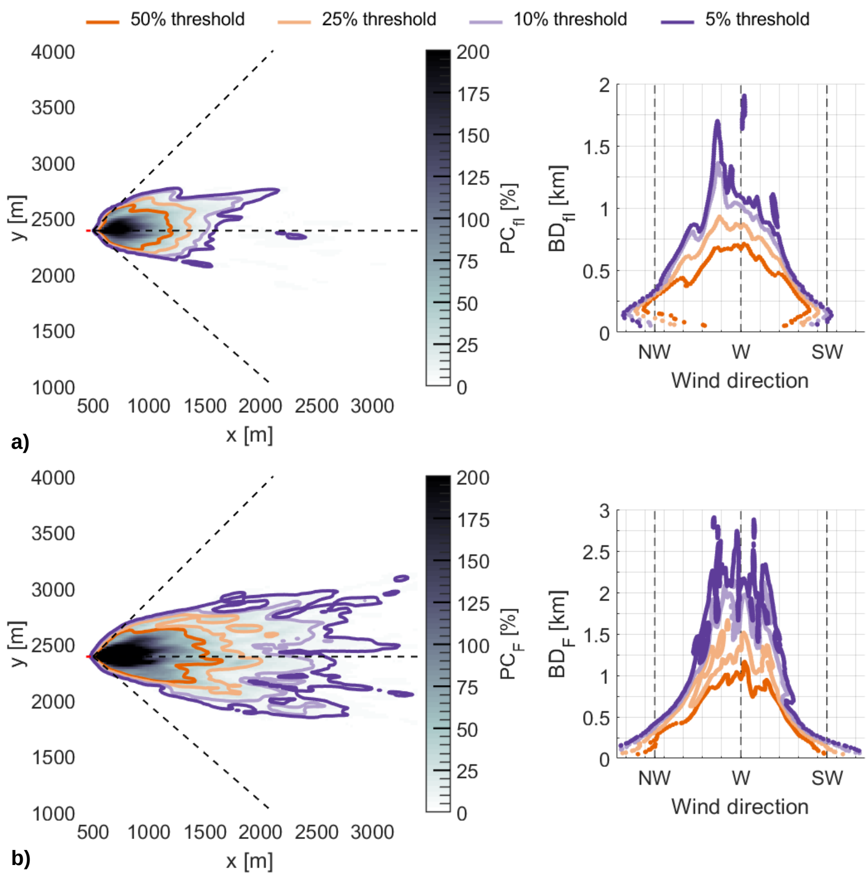

Figure 5. The left panels show the spatial structure of the percentage change in grayscale for the fluctuation intensity (PC_{fI}) in (a) and the ammonia flux (PC_F) in (b). The colored contour lines show the locations where the 50% (orange), 25% (light orange), 10% (light-purple) and 5% (purple) thresholds are met, representing the blending-distance (BD). The right panels show these blending-distances as a function of different angles from the plume centerline (W), with these angles representing the wind direction.

We interpret the calculation of the blending-distance based on ~~3 arbitraty~~ 4 arbitrary threshold levels (5%, 10%, 25% and 50%) for fI and F, shown in Fig. 4a and b. The distance at which the maximum value of PC_X drops below the threshold level is the blending-distance. The sensitivity of BD to these thresholds will be discussed in detail in Sect. 4.1, using Fig. ~~?? and ??~~6 and 7. Additionally, ~~we show~~ the intermittency in Fig. 4c ~~to show~~ shows that the emission plume is ~~quantifyable~~ quantifiable up to over ~~2.6~~ 2.4 km distance.

Starting with the fluctuation intensity (Fig. 4a), PC_{fI} peaks at a relative change of about 300%, caused by the NH_3 emission plume. BD_{fI} decreases non-linearly from ~~1.5 km to 1~~ 0.7 km to 1.9 km with the thresholds ~~increasing from 5% to 25%. We can therefore infer from BD_{fI} that, while the NH_3 plume is still quantifiable, the change in fluctuation intensity caused by the plume is <~~ decreasing from 50% to 5%~~at 1.5 km or less, depending on wind direction.~~

. Figure 4b shows that the emission plume has a larger impact on NH_3 flux measurements than on ~~measurements~~ the fluctuation intensity of the NH_3 molar fraction. The large difference between the emission strenght (45 ppb m s^{-1}) and the deposition (-0.045 ppb m s^{-1}) result in a maximum PC_F of ~~nearly 750~~about 1200% in close proximity of the emission source~~and a long tail , indicating that the emission plume affects~~ . The long tail of PC_F indicates that the turbulent fluctuations in the emission plume affect flux measurements over several kilometers. As a result, BD_F ~~decreases from 2.9 km to 1.4 km for increasing~~ increases from 1.2 km to 2.9 km for decreasing thresholds, significantly longer distances then our 1 km qualitative estimate based on Fig. 3d. ~~The fluctuations in F_{bg}, shown in Fig. 3d, translate to fluctuations in PC_F, as shown in the zoomed panel of Fig. 4b.~~ Note that Fig. 3d shows that the flux changes sign in proximity of the emission source and that this sign change is not reflected in Fig. 4b.

Figure 4 shows that the centerline and the maximum statistics give similar results, indicating that the highest values of PC are found at the plume centerline, though with some variability. These variabilities are visualized in Fig. 5, which shows the spatial structure of the percentage change in grayscale for the fluctuation intensity (PC_{fI}) in (a) and the ammonia flux (PC_F) in (b). The colored lines in these panels represent the blending-distances for different thresholds. The right panels show these same blending-distances for different angles from the plume centerline (W), representing different wind directions. Fig. 5 shows large variability in the blending-distance, especially for the 5% and 10% threshold levels, as a result of the chaotic nature of turbulence.

4 Discussion

4.1 Sensitivity of blending-distance to meteorological and NH_3 pollution variables

We study the sensitivities of BD_{fI} and BD_F to a range of meteorological, NH_3 pollution parameters and model resolution and simulated measurement height (Table 1). The results of the sensitivity study are shown in Fig. ~~?? and ??~~ 6 and 7 for an arbitrary set of threshold ranging from 5% (orange dashed) to 50% (orange dotted), representing the maximum acceptable difference in fI and F caused by the emission plume in %.

Starting with BD_{fI}, Fig. ~~??~~ 6 shows that BD_{fI} ranges roughly between 0.5 and ~~2.5 km; an indicating~~ 3.0 km; a first-order estimate of the minimum ~~distence~~ distance for NH_3 molar fraction measurements. There is a negative correlation between BD_{fI} and the choice in threshold, i.e. increasing the threshold level decreases BD_{fI}. We generally find that BD_{fI} decreases nonlinearly by approximately ~~0.5~~ 1.0 km when increasing the threshold level from ~~5~~10% to 50%, halving BD_{fI}, highlighted by the large difference between the 10% (dashed-dotted) and 5% (dashed) threshold levels for both BD_{fI} and BD_F. We discuss the individual variables of Fig. ~~??~~ 6 from top to bottom, starting at the mesoscale (u_g), down to the micrometer scale (R) and finishing with the model resolution and simulated measurement heigth.

The geostrophic wind speed (u_g) is one of the main drivers of turbulent mixing and transport of the plume (Dosio et al., 2003; Vrieling and Nieuwstadt, 2003; Dosio and Vilà-Guerau de Arellano, 2006). Figure ~~?? shows that BD_{fI} is only weakly sensitive to u_g, showing a weak~~ 6 shows a positive correlation between ~~the two~~BD_{fI} and u_g. By varying u_g we move from a convection-driven boundary layer (u_g = 2 m s^{-1}) to more shear-driven meteorological conditions (u_g = 10 m s^{-1}). In a convection-driven

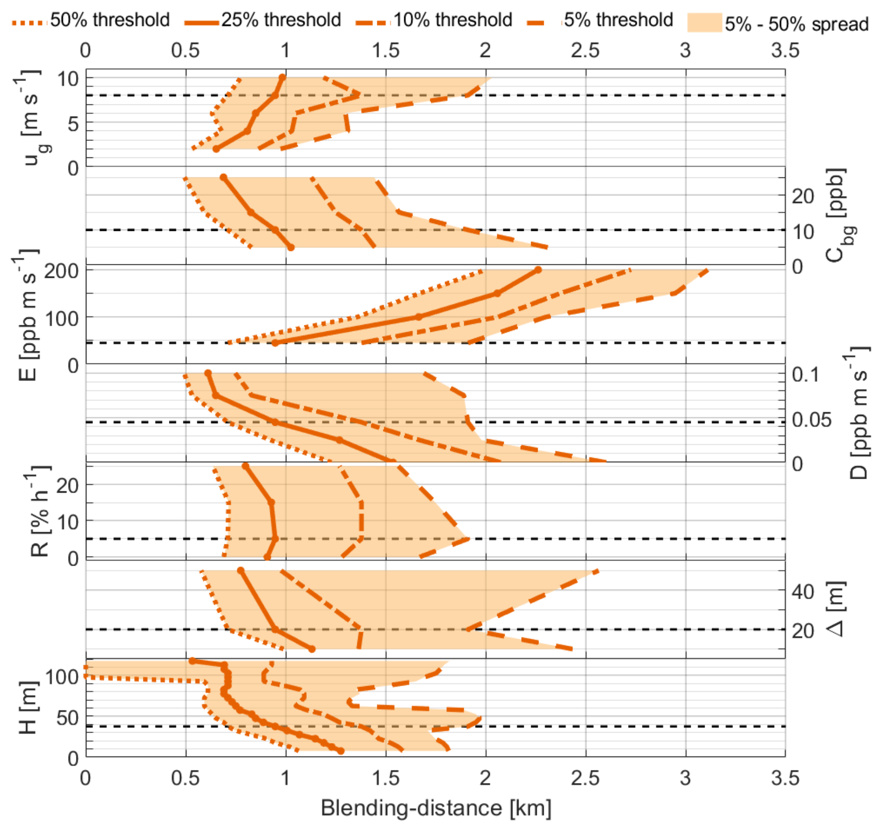

Figure 6. The sensitivity of BD_{fI} to the geostrophic wind speed (u_g), initial background molar fraction (C_{bg}), emission strength (E), deposition ~~strenght~~ strength (D), chemical reaction rate (R), model resolution (Δ) and simulated measurement height (H). BD_{fI} is determined for threshold levels ranging from 5% (orange dashed) to 50% (orange dotted).

boundary layer, turbulent mixing is rather weak and the NH_3 emission plume rises from the surface as convection plumes are the main drivers of turbulent mixing. Under these conditions, in-plume molar fractions are very high, but horizontal transport of the emission plume is weak, resulting in a low BD_{fI}. For shear-driven conditions, the NH_3 emission plume tends to stick to the surface as the increased horizontal wind speed enhances horizontal transport and turbulent mixing. The enhanced horizontal transport and emission plume sticking to the surface should significantly increase BD_{fI}, but the enhanced turbulent mixing counteracts these processes by reducing the $NH_{3,plume}$ molar fraction and fluctuations. This is ~~exactly what is~~ shown in Fig. ~~??~~ 6 and explains why the sensitivity of BD_{fI} increases for lower threshold levels (5%), as smaller plume fluctuations will reach long ~~dinstances~~ distances in shear-driven conditions.

One panel below, Fig. ~~?? shows a weak~~ 6 shows a negative correlation between BD_{fI} and the initial background molar fraction (C_{bg}), i.e. the regional level of NH_3 pollution. ~~Increasing C_{bg} enhances the fluctuations in the CBL by entrainment, increaing~~ The first cause of the negative correlation is the higher average molar fraction, which lowers relative weight of the $NH_{3,plume}$ fluctuations (σ_{plume}) when fI_{total} is calculated following Eq. 2. Additionally, increasing $NH_{3,bg}$ leads to a large difference in the NH_3 air mass characteristics at the top of the boundary-layer. The exchange between the boundary layer and free tropospheric air masses throught entrainment increases σ_{bg} at 37.5 m from 0.13 ppb (C_{bg} = 5 ppb) to 0.38 ppb (C_{bg} = 25 ppb)~~. The relative weight of the NH~~, resulting in an increased fI_{bg}. Both processes reduce the magnitude of $PC_{~~3,plume~~fI}$ ~~fluctuations (~~~~σ~~with increasing C~~plume) decreases as a result, leading to slightly lower~~$_{bg}$, reducing BD_{fI}.

At the local scale, Fig. ~~??~~ 6 shows a clear positive and negative correlation when varying emission strength (E) and deposition strength (D) respectively. Both variables directly affect one of the main drivers of turblent mixing: heterogeneity. Increasing the NH_3 emission strength of the local (heterogeneous) source directly increases fI_{plume}, increasing BD_{fI}. Varying the deposition on the other hand, directly affects the vertical gradient of the NH_3 molar fraction ~~gradient~~ near the surface, increasing fI_{bg} for increasing D and therefore reducing BD_{fI}.

We only briefly touch upon the chemical conversion rate (R), as Fig. ~~??~~ 6 shows that varying R does not significantly affect BD_{fI}. R is applied uniformly to the 3D domain and has little effect on turbulent mixing. Note that our simplified representation of chemistry could lead to a potential underestimation of the impact of chemistry on BD_{fI}, as our approach is unable to resolve potential non-linear effects of turbulent mixing on the in-plume chemical reaction rate near the emission source (see discussion in Sect. 4.1).

Next, we vary the model resolution (Δ) in Fig. ~~??~~ 6 and find that BD_{fI} is weakly sensitive to the model resolution. ~~While the smallest fluctuations are not resolved by the model at Δ = 20 x 20 x 5 m, the weak sensitivity of BD_{fI} indicates that this resolution is sufficient to infer the~~ The results indicate that the calculation of the blending-distance does benefit by increasing the simulation resolution. However, there is a trade-off between the computational costs of the simulation and the resolution.

Finally, Fig. ~~??~~ 6 shows two regimes in the sensitivity of BD_{fI} to the simulated measurement height (H). For the 50% threshold, BD decreases by about ~~300~~ 500 m with height up to ~~60~~ 90 m. Above ~~60~~ 90 m, there is a transition where BD_{fI} rapidly goes to zero. In this second regime, the simulated measurements are located above the plume ~~centreline~~centerline. From there on, fI_{plume} rapidly decreases with height until PC_{fI} does not reach the 50% threshold and BD_{fI} becomes zero. This rapid decrease is a result of the ~~similated~~ simulated measurements being located above the emission plume, as the height of plume does not reach above 150 m for the first 1.5 km horizontal distance. The height of this transition increases with decreasing threshold levels as the thresholds become more sensitive to smaller $NH_{3,plume}$ fluctuations.

Figure ~~??~~ 7 shows the results of the sensitivity study for BD_F (Table 1). Both the blending-distance for molar fraction measurements (BD_{fI}) and for flux measurements (BD_F) can be interpreted as a inverse footprint analysis, as we estimate the area affected by the emission source. The results of the sensitivity study of BD_F however, ~~could differ from the sensitivity study of BD_{fI} . The~~ are different from the BD_{fI} results, as the footprints for flux and molar fraction measurements are not the same~~and footprint~~. Footprint for flux measurements are smaller than those of molar fraction measurements (Rannik et al., 2000; Kljun et al., 2003; Vesala et al., 2008). However, comparing BD_{fI} to the footprint of NH_3 molar fraction measurements is not straightforward, as BD_{fI} is based on the NH_3 fluctuation intensity, not the molar fraction. It is therefore interesting to determine whether the results of the sensitivity study of BD_F will differ compared to the results of BD_{fI}.

When analyzing Fig. ~~??~~7, we find that there are indeed differences between BD_F and BD_{fI}. BD_F is significantly longer, ranging from ~~1.0 to 3.5~~ 0.75 to roughly 5 km, indicating that NH_3 flux measurements are more sensitive to the emission plume.

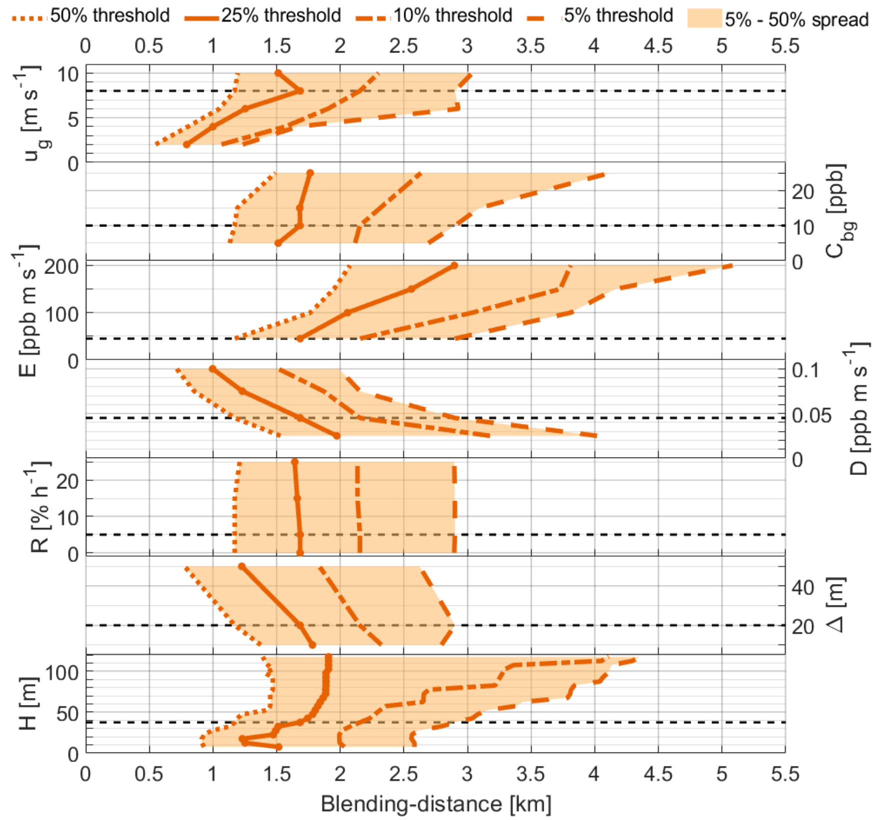

Figure 7. The sensitivity of BD_F to the geostrophic wind speed (u_g), initial background molar fraction (C_{bg}), emission strength (E), deposition ~~strenght~~ strength (D), chemical reaction rate (R), model resolution (Δ) and simulated measurement height (H). BD_F is determined for threshold levels ranging from 5% (orange dashed) to 50% (orange dotted).

Note that we removed the results for D = 0 ppb m s^{-1}. Here, F_{bg} approaches zero, resulting in infinitely large PC_F and unrealistic BD_F values~~.~~ , following Eq. 6.

One of main differences between BD_F and BD_{fI} are found in the sensitivity to the threshold levels (5% to 50%). BD_F is more sensitive to the different threshold levels compared to BD_{fI}. This is in agreement with the results shown in Fig. 4b, where we discussed that PC_F is significantly larger than PC_{fI}, with a ~~significanlty longer tailas well. Despite these differences, the same arbitrary set of thresholds are used for both BD_{fI} and BD_F~~longer tail. As a result, the non-linear effect of the aforementioned long tail in PC_F (Fig. 4b) increases BD_F for low threshold levels. Despite these differences, the same arbitrary set of thresholds are used for both BD_{fI} and BD_F.

Significant differences between BD_F and BD_{fI} are also found in the sensitivity to the geostrophic wind speed (u_g) and the simulated measurement height (H). Both variables directly affect the footprint of the simulated flux measurements. In shear-driven turbulent conditions (high u_g), the footprint of the measurement is elongated compared to convective conditions. This reduces the width of the footprint and lengthens the up-wind distance at which the emission source can be measurement, thus increasing BD_F. Increasing H also increases the footprint of the measurements, but there is no elongation of the footprint. As a result, BD_F has a strong positive correlation to u_g but is only weakly correlated to H, except for the lower threshold levels.

Fig. 7 appears to show that BD_F has a weak positive correlation with increasing C_{bg}. This is mainly attributed to an increase in the spatial variations of the background NH_3 flux, which increases from $\sigma_{F,bg}$ = 0.0065 ppb m s^{-1} for C_{bg} = 10 ppb (Fig. 3d) to $\sigma_{F,bg}$ = 0.015 for C_{bg} = 25 ppb. As a result, the fluctuations in PC_F shown in Fig. 4b increase in amplitude and frequency which particularly affects the low threshold levels of 5% and 10% .

There are also strong similarities between the sensitivity of BD_F and BD_{fI}. Both Fig. ~~?? and ??~~ 6 and 7 show that the blending-distance is only weakly sensitive to the chemical reaction rate (R) ~~, initial background molar fraction (C_{bg}) and to~~ and the model resolution (Δ). For both molar fraction and flux measurements, the emission strength (E), deposition (D) and to a lesser extent the geostrophic wind speed (u_3 are the driving variables of the blending-distance.

5 ~~Discussion~~

4.1 Uncertainty ~~on~~ of the blending-distance estimation

The ~~blending-distance cannot be captured by a single number. The~~ turbulent dispersion of the emission plume is chaotic by nature and driven by a wide range of factors. We therefore carry out a systematic analysis on how these factors, as well as the model resolution, influence the the relationships between emission and the simulated in-field measurements. ~~Additionally, the~~ The chaotic nature of turbulence ~~introduces~~ results in random variations in both the emitted NH_3 (Fig. 3a and b) and the background NH_3 (Fig. 3c and d). These random fluctuations lead to variability in the calculation of the blending-distances, leading to uncertainty in the blending-distances presented in this study~~, .~~. The variability increases when using the lower threshold levels (e.g. 5% and 10%), as is visualized and discussed in Sect. 3.1 ~~, where random spatial variabilityis seen in the fluctuation intensity and flux of $NH_{3,bg}$. This introduces an uncertainty in the blending-distance which is especially pronounced in the analysis of the NH_3 flux, as discussed in Sect. 3.2~~and 3.2. The variability could be reduced by increasing the length of the analysis window, i.e. increasing the averaging time to filter out the small and short spatio-temporal turbulence variability.

~~Furthermore~~Increasing the length analysis window however, means that the blending-distance is calculated using a wider range of boundary layer dynamics and variations in the thermodynamic variables. Boundary layer dynamics are especially relevant in the morning and early afternoon, when the boundary-layer grows and air from the residual layer and free troposphere is entrained, or in the afternoon when turbulence decays (Pino et al., 2006). It leads to entrainment being one of the dominant processes driving the NH_3 diurnal variability (Wichink Kruit et al., 2007; Schulte et al., 2021). We show in Fig. 2 it leads leads to large fluctuations in $NH_{3,bg}$, significantly increasing fI_{bg}. We therefore filter out the impact of boundary layer dynamics and variations in the thermodynamic variables with our choice of analysis window from 14:00 and 17:00 CEST, in order to find a first-order estimate of the blending-distance. We do recommend a follow-up study on the role of boundary dynamics.

Finally, there is a downside to of our simplified representation of chemical transformations, in that it is applied uniformly to the 3D domain. In reality, the equilibrium molar fractions for these chemical transformations are related to temperature and humidity and results in a near-surface NH_3 gradient of the NH_3 molar fraction (aan de Brugh et al., 2013). Therefore, we are likely to underestimate the role of chemical transformations and overestimate BD_{fI}, as turbulent mixing of this near-surface gradient increases fI_{bg}.

~~Finally, we filter out the impact of boundary-layer dynamics and variations in~~ The blending-distance cannot be captured by a single number. This is partly due to the uncertainty involved in calculating the blending-distance, but the blending-distances is most of all an integrated variable. Several processes are captured by the blending-distance in one single variable, including the chaotic nature of turbulent plume dispersion, convective and shear induced turbulence, atmospheric pollution levels and surface heterogeneity. As shown in Sect. 4.1, each of these processes impacts the blending-distance differently. Despite its complexity, the ~~thermodynamic variables with our choice of analysis window, from 14:00 and 17:00 CEST. Bourndary-layer dynamics are especially relevant in the morning, when entrainment is one of the dominant processes driving the NH_3 diurnal variability (Wichink Kruit et al., 2007; Schulte et al., 2021). As shown in Fig. 2, entrainment leads to large fluctuations in $NH_{3,bg}$, increasing fI_{bg} and leading to a shorter BD_{fI}. Despite these uncertainties~~blending-distance is a useful variable since it is an integrated variable; all the aforementioned processes are represents in this distance at which the impact of an emission plume is negligible with respect to the background.

The applicability of the results presented here depend not only on the meteorological and NH_3 pollution factors, but also on the physical context of the measurement site. This study is based on the Ruisdael CESAR Observatory at Cabauw, which is located on flat agricultural grassland with surface elevation changing only by a few meters over 20 km. A different physical context, like a heterogeneous surface which changes the turbulent properties (Ouwersloot et al., 2011), is likely to significantly affect the resulting blending-distances. With the simulation framework presented here, the blending-distance ~~provides a valuable first esitmate for the minimum distance required for measurements taken in proximity of a typical NH_3 emission source.~~ can be calculated for specific weather conditions and for the physical context of the measurement site, providing a more accurate assessment of the impact of nearby emissions on NH_3 observations at a specific measurement site. The results presented in this study provide a valuable first estimate of, and discussion on, a typical blending-distance and its driving variables.

4.2 Blending-distance literature for passive tracers

Evaluating the blending-distance results against typical literature on plume dispersion is a ~~complex exercise. These studies generally~~ difficult exercise. The topic is generally not mentioned as these studies focus on the release of passive scalars in an unpolluted environment ~~, with~~ and only few studies ~~researching~~ even research (near) surface releases (Cassiani et al., 2020). Normalization of both distance from the source ~~as the plume~~ and the in-plume molar fraction further complicates the interpretation of literature ~~. We can make a rough estimate of~~ results.

We therefore try to estimate the order of magnitude of the blending-distance ~~, using the modelled~~ based on the in-plume molar fraction and fluctuation intensity of plume dispersion modeling studies. Following figures by Dosio et al. (2003) and Dosio and Vilà-Guerau de Arellano (2006), ~~which~~ we find that the in-plume molar fraction rapidly decreases for a convection-driven boundary layer ($-z/L \geq 40$ and $u_*/w_* \leq 0.2$) at the surface up to roughly 6 km distance, after which it ~~levels off. This~~ starts to level off. Similar results are found for the fluctuation intensity, although the results are less pronounced for the near-surface release experiments. The 6 km distance approximately doubles for shear-driven boundary layers ($-z/L \sim 40$ and $u_*/w_* \sim 0.46$). The observations by Mylne and Mason (1991) and the large-edy simulation results of Dosio et al. (2003) shown in Figure 10 by Mylne and Mason (1991) show that the in-plume observed fluctuation intensity also decreases with distance, but levels after roughly 15 km distance from the emission source. We use these distances at which the plume statistics start to level off as an estimate of the order of magnitude of the blending-distance, indicating that the blending-distance could be in the order of several kilometers (6 to 15 km), based on plume dispersion literature.

These rough estimates of 6 to 15 km distance are significantly larger than the blending-distances presented in this study. Such long distances between source and measurement site would not make feasible requirements in densely agricultural regions, but are likely an overestimation of the blending-distance. These estimates are based on the molar fraction and fI of the emission plume, with no representation of background ammonia levels. The latter is especially important, as we show in Sect. 3.1 and 3.2 that the impact of the emission plume rapidly decreases relative to the turbulent background ammonia, while the emission plume itself can be detected for several kilometers as indicated by the intermittency.

4.3 Blending-distance literature for ammonia measurements

Articles on ammonia measurements in close proximity of an emssion emission source implicitly include all relevant processes. Such studies could also provide a qualitative, perhaps more realistic, evaluation of the NH_3 blending-distance results presented here. In-field measurements show that the NH_3 molar fraction exponentially decreases with distance from the source, with measurements close to the background molar fraction after 300 to 500 m (Fowler et al., 1998; Sommer et al., 2009; Shen et al., 2016). Similar results were obtained in an intercomparison study of short-range atmospheric dispersion models by Theobald et al. (2012), at horizontal resolutions of 25 - 50 m and receptors at 100 m intervals along four radial directions (N, E, S and W). However, such measurements are typically arranged in a few lines downwind of the source, with only a handful of measurements over a distance of 300 to 1000 m. At these short distances, plume dispersion is dominated by meandering of the plume (Nieuwstadt, 1992) and the in-plume molar fraction measurements are underestimated as a result, especially given the averaging times of these measurements ranging from several hours up to multiple weeks.

Finally, we can evaluate our findings against measurement site requirements of air quality networks. The Dutch air quality network and the EMEP (European Monitoring and Evaluation Programme) network do set requirements on the minimum distance from emission sources, no references to scientific studies are provided. Back in 1990, the Dutch network required a minimum distance for NH_3 sites of 300 - 500 m from NH_3 point or area sources, depending on source strength (Boermans and Erisman, 1990). This is in line with the literature on measurements in proximity of emission sources discussed earlier, but closer than the blending-distances presented here. Currently, no hard requirements are in place in the Netherlands, although the potential impact of NH_3 sources is still recognized (Wichink Kruit et al., 2021). At a European level, EMEP measurement sites require a 2 km minimum distance for measurements nearby stabling of animals and manure application, depending on the number of animals and field size (Schaug, 1988; EMEP/CCC, 2001). This 2 km distance is in line with our recommendations. However, the blending-distance presented , although the results in this study indicate that distances below 2 km could also be sufficientto assure the measurement site to be regionally representative.

4.4 Towards an NH_3 virtual testbed: integrating fine-scale simulations with advanced observations

This study is the first which specifically addresses the regional representativity of ammonia measurements in proximity of an emission source. The systematic analysis presented in Fig. ?? and ?? 6 and 7 can be used as a reference when interpreting in-field NH_3 measurements. Additionally, the simulation framework can be applied for to individual locations and study the representativity of (potential new) measurement sites under the local conditions, using the concept of blending-distance. The framework presented here can be expanded One can expanded the simulation framework to include multiple sources, area sources, each with an unique passive scalar, as well as heterogeneous surface conditions (Ouwersloot et al., 2011), to simulate the local NH_3 conditions.

The DALES model has proven to be flexible, allowing for simulations of a convective, sheared convective, stable and cloud topped boundary layer (Verzijlbergh et al., 2009; Heus et al., 2010). The fine scale fine-scale simulation framework will be included in the Ruisdael ObservatoryCESAR Observatory at Cabauw (https://ruisdael-observatory.nl), a nationwide observatory for measurements and modelling modeling of the atmosphere and air quality, but can be used at any location where topography does not play an important role. The simulation framework . It can be a powerful tool in future ammonia research, e.g. in preparation of (emission) measurement campaigns or to improve interpretation of NH_3 (flux) measurements. Furthermore, we want to stress that the simulation framework is methods presented here are not limited to ammonia, but can be used for any gas for which the relevant processes occur at high spatio-temporal resolution. The fine scale simulation framework will be included in the Ruisdael Observatory (), a Dutch nationwide observatory for measurements and modelling of the atmosphere and air quality, but can be used at any location where topography does not play an important role.

We recommend to expand the simulation framework to create a testbed to study NH_3 at high spatio-temporal resolution, including all processes relevant to the NH_3 diurnal variability. The main additions should be a dynamic parameterization of the surface-atmosphere exchange, e.g. DEPAC (van Zanten et al., 2010), and a thermodynamic chemistry module, e.g. ISORROPIA version 2 (Fountoukis and Nenes, 2007). With these additions, on top of the existing possibility to distinguish between background and emitted NH_3, the fine scale fine-scale simulation framework with explicitly resolved turbulence will be well suited to study short-range dispersion of ammonia, e.g. deposition in close proximity to emission sources and the impact of turbulent micromixing on the chemical reaction rate. Such studies are typically performed using models where turbulence is parameterized or using Gaussian plume models (Loubet et al., 2006; Sommer et al., 2009; van der Swaluw et al., 2017). Furthermore, the addition of a thermodynamic chemistry module can lead to new insights on NH_3 flux measurements. The equilibrium molar fractions of the NH_3 gas-aerosol transformations depend on the atmospheric temperature and humidity, resulting in a near-surface molar fraction gradient. This gradient leads to an underestimation of the NH_3 deposition flux of about 0.02 $\mu g\ m^{-2} s^{-1}$ when using the flux-gradient method (Nemitz et al., 2004). With these additions to the simulation framework, the virutal NH_3 testbed can be used improve the interpretation of NH_3 flux measurements.

5 Conclusions

This paper presents a ~~fine scale~~ fine-scale simulation framework with which we assess the regional representativity of NH_3 molar fraction and flux measurements in proximity of a typical NH_3 emission source. We aim to translate concepts from the fields of plume dispersion and ~~fine scale simulations to a practical application in the field~~ fine-scale simulations to support the analysis of NH_3 ~~measurements~~observations in areas characterized by NH_3 (point) source emissions, including realistic representations of NH_3 surface-atmosphere exchange and chemical gas-aerosol transformations. The concept of a blending-distance is introduced to systematically analyze the impact of the emitted NH_3 on simulated measurements, relative to a background concentration. Following this approach, we define a first-order estimate of a minimum distance requirement between regional representative measurements and a typical NH_3 emission source.

By means of ~~fine scale~~ fine-scale simulation of atmospheric NH_3, we investigate the representativity of NH_3 measurements from kilometer to meter scales in proximity of a typical emission source. The ~~fine scale~~ fine-scale simulation framework presented has proven to be a powerful and flexible tool for future research on ammonia, or any gas for which the relevant processes occur at high spatio-temporal resolution. The simulation framework with explicitly resolved turbulence not only enables us to quantify the variability in NH_3 measurements, but also to analyze and quantify the individual contribution of the ~~emitted NH_3~~ NH_3 emission plume. The concept of blending-distance presents a consistent ~~criterium~~criterion, based on second order statistics, for the minimum distance at which the impact of the emitted NH_3 is estimated to be indistinguishable from the variability of the background NH_3. ~~A systematic analysis~~ Following this approach, we perform several numerical experiments to analyze the sensitivity of the blending-distance to a variety of meteorological and NH_3 pollution variables, centered around the flat grassland at Ruisdael CESAR Observatory at Cabauw. This systematic analysis shows a strong sensitivity to the emission ~~strenght~~strength, deposition and the threshold level used in the calculation, and to the stability of the (convective or shear dominated) boundary layer. Furthermore, we find that the blending-distances differ for NH_3 molar fraction and flux measurements, with flux measurements being more sensitive to the NH_3 emission plume. Following this sensitivity analysis, we conclude that NH_3 measurements at the CESAR Observatory should be taken at a minimum distance of 0.5 - ~~2.5 km or 1~~ 3.0 km or 0.75 - ~~3.5~~ 4.5 km distance from an emission source, for measurements of the NH_3 molar fraction or flux respectively.

Code availability. Model code and processing scripts will be made availabile upon publication.

Author contributions. RS and JV worked on the conceptualization and developed the methodology of the numerical experiments. RS and BS made modifications to the software, i.e. the DALES model. The numerical experiments were performed by RS, who also analyzed and visualized resulting data. The manuscript draft is written by RS and reviewed by both JV and MZ. Finally, the project was supervised by JV and MZ.

Competing interests. The authors declare that they have no conflict of interest.

Acknowledgements. We thank Bart van Stratum (WUR) for his assistance with setting-up the DALES model and for his support with the modifications of the model. This research was financed by the Dutch National Institute of Public Health and the Environment (RIVM) within the framework of the Project 36.7: Monitoring of dry ammonia deposition, which is performed by order, and for the account, of the Dutch Ministry of Agriculture, Nature and Food Quality. The numerical simulations were performed with the supercomputer facilities at SURFsara and financially sponsored by the Netherlands Organisation Organization for Scientific Research (NWO) Physical Science Division (project number 2021/ENW/01081379).

References

aan de Brugh, J. M. J., Henzing, J. S., Schaap, M., Morgan, W. T., van Heerwaarden, C. C., Weijers, E. P., Coe, H., and Krol, M. C.: Modelling the partitioning of ammonium nitrate in the convective boundary layer, Atmospheric Chemistry and Physics, 12, 3005–3023, https://doi.org/10.5194/acp-12-3005-2012, 2012.

aan de Brugh, J. M. J., Ouwersloot, H. G., Vilà-Guerau de Arellano, J., and Krol, M. C.: A large-eddy simulation of the phase transition of ammonium nitrate in a convective boundary layer, Journal of Geophysical Research: Atmospheres, 118, 826–836, https://doi.org/10.1002/jgrd.50161, 2013.

Anys, M., Ullrich, B., Gager, M., and Pinterits, M.: European Union emission inventory report 1990-2018: under the UNECE Convention on Long-range Transboundary Air Pollution, Tech. Rep. TH-AL-20-013-EN-N, European Environment Agency, Kongens Nytorv 6, 1050 Copenhagen K, Denmark, https://www.eea.europa.eu/ds_resolveuid/c48fe5a189e5484095dcb509da927a36, 2020.

Ardeshiri, H., Cassiani, M., Park, S. Y., Stohl, A., Pisso, I., and Dinger, A. S.: On the Convergence and Capability of the Large-Eddy Simulation of Concentration Fluctuations in Passive Plumes for a Neutral Boundary Layer at Infinite Reynolds Number, Boundary-Layer Meteorology, 176, 291 – 327, https://doi.org/10.1007/s10546-020-00537-6, 2021.

Barad, M. L.: Project Prairie Grass, a field program in diffusion. Volume 1, Tech. Rep. No. 59, Vol I , Report AFCRC-TR-58-235(I), AIR FORCE CAMBRIDGE RESEARCH LABS, https://www.harmo.org/jsirwin/PGrassVolumeI.pdf, 1958.

Barbaro, E., Vilà-Guerau de Arellano, J., Ouwersloot, H. G., Schröter, J. S., Donovan, D. P., and Krol, M. C.: Aerosols in the convective boundary layer: Shortwave radiation effects on the coupled land-atmosphere system, Journal of Geophysical Research: Atmospheres, 119, 5845–5863, https://doi.org/10.1002/2013JD021237, 2014.

Barbaro, E., Krol, M., and Vilà-Guerau de Arellano, J.: Numerical simulation of the interaction between ammonium nitrate aerosol and convective boundary-layer dynamics, Atmospheric Environment, 105, 202–211, https://doi.org/10.1016/j.atmosenv.2015.01.048, 2015.

Behera, S. N., Sharma, M., Aneja, V. P., and Balasubramanian, R.: Ammonia in the atmosphere: a review on emission sources, atmospheric chemistry and deposition on terrestrial bodies, Environmental Science and Pollution Researc, 20, 8092 – 8131, https://doi.org/10.1007/s11356-013-2051-9, 2013.

Berkhout, A. J. C., Swart, D. P. J., Volten, H., Gast, L. F. L., Haaima, M., Verboom, H., Stefess, G., Hafkenscheid, T., and Hoogerbrugge, R.: Replacing the AMOR with the miniDOAS in the ammonia monitoring network in the Netherlands, Atmospheric Measurement Techniques, 10, 4099–4120, https://doi.org/10.5194/amt-10-4099-2017, 2017.

Boermans, G. M. F. and Erisman, J. W.: Meetstrategieontwikkeling voor het representativiteitsonderzoek als onderdeel van het additioneel meetprogramma ammoniak: fenomenologie van NH3 en meetritsimulaties, Tech. Rep. 222105001, National Institute for Public Health and the Environment (RIVM), Antonie van Leeuwenhoeklaan 9, 3721, MA Bilthoven, the Netherlands, http://hdl.handle.net/10029/255566, 1990.

Cassiani, M., Bertagni, M., Marro, M., and Salizzoni, P.: Concentration Fluctuations from Localized Atmospheric Releases, Boundary-Layer Meteorology, 177, 461–510, https://doi.org/10.1007/s10546-020-00547-4, 2020.

Dosio, A. and Vilà-Guerau de Arellano, J.: Statistics of Absolute and Relative Dispersion in the Atmospheric Convective Boundary Layer: A Large-Eddy Simulation Study, Journal of the Atmospheric Sciences, 63, 1253 – 1272, https://doi.org/10.1175/JAS3689.1, 2006.

Dosio, A., Vilà-Guerau de Arellano, J., Holtslag, A. A. M., and Builtjes, P. J. H.: Dispersion of a Passive Tracer in Buoyancy- and Shear-Driven Boundary Layers, Journal of Applied Meteorology, 42, 1116 – 1130, https://doi.org/10.1175/1520-0450(2003)042<1116:DOAPTI>2.0.CO;2, 2003.

EMEP/CCC: EMEP manual for sampling and chemical analysis, Tech. Rep. EMEP/CCC-Report 1/95, O-7726, Chemical Co-ordination Centre of EMEP (EMEP/CCC), https://projects.nilu.no/ccc/manual/download/cccr1-95rev.pdf, 2001.

Erisman, J. and Schaap, M.: The need for ammonia abatement with respect to secondary PM reductions in Europe, Environmental Pollution, 129, 159–163, https://doi.org/10.1016/j.envpol.2003.08.042, 2004.

Erisman, J. W., Galloway, J. N., Seitzinger, S., Bleeker, A., Dise, N. B., Petrescu, A. M. R., Leach, A. M., and de Vries, W.: Consequences of human modification of the global nitrogen cycle, Philosophical Transactions of the Royal Society B: Biological Sciences, 368, 20130 116, https://doi.org/10.1098/rstb.2013.0116, 2013.

Fountoukis, C. and Nenes, A.: ISORROPIA II: a computationally efficient thermodynamic equilibrium model for K^+-Ca^{2+}-Mg^{2+}-NH_4^+-Na^+-SO_4^{2-}-NO_3^--Cl^--H_2O aerosols, Atmos. Chem. Phys., 7, 4639–4659, https://doi.org/10.5194/acp-7-4639-2007, 2007.

Fowler, D., Pitcairn, C. E. R., Sutton, M. A., Flechard, C., Loubet, B., Coyle, M., and Munro, R. C.: The mass budget of atmospheric ammonia in woodland within 1 km of livestock buildings, Environmental Pollution, 102, 343 – 348, https://doi.org/10.1016/S0269-7491(98)80053-5, 1998.

Gailis, R. M., Hill, A., Yee, E., and Hilderman, T.: Extension of a fluctuating plume model of tracer dispersion to a sheared boundary layer and to a large array of obstacles, Boundary-Layer Meteorology, 122, 577–607, https://doi.org/10.1007/s10546-006-9118-9, 2007.

Galmarini, S., Vilà-Guerau de Arellano, J., and Duynkerke, P.: The effect of micro-scale turbulence on the reaction rate in a chemically reactive plume, Atmospheric Environment, 29, 87–95, https://doi.org/10.1016/1352-2310(94)00224-9, 1995.

Heus, T., van Heerwaarden, C. C., Jonker, H. J. J., Pier Siebesma, A., Axelsen, S., van den Dries, K., Geoffroy, O., Moene, A. F., Pino, D., de Roode, S. R., and Vilà-Guerau de Arellano, J.: Formulation of the Dutch Atmospheric Large-Eddy Simulation (DALES) and overview of its applications, Geoscientific Model Development, 3, 415–444, https://doi.org/10.5194/gmd-3-415-2010, 2010.

Kljun, N., Kormann, R., Rotach, M. W., and Meixer, F. X.: Comparison of the lagrangian footprint model LPDM-B with an analytical footprint model, Boundary-Layer Meteorology, 106, 349–355, https://doi.org/10.1023/A:1021141223386, 2003.

Kulmala, M., Asmi, A., Lappalainen, H. K., Baltensperger, U., Brenguier, J.-L., Facchini, M. C., Hansson, H.-C., Hov, Ø., O'Dowd, C. D., Pöschl, U., Wiedensohler, A., Boers, R., Boucher, O., de Leeuw, G., Denier van der Gon, H. A. C., Feichter, J., Krejci, R., Laj, P., Lihavainen, H., Lohmann, U., McFiggans, G., Mentel, T., Pilinis, C., Riipinen, I., Schulz, M., Stohl, A., Swietlicki, E., Vignati, E., Alves, C., Amann, M., Ammann, M., Arabas, S., Artaxo, P., Baars, H., Beddows, D. C. S., Bergström, R., Beukes, J. P., Bilde, M., Burkhart, J. F., Canonaco, F., Clegg, S. L., Coe, H., Crumeyrolle, S., D'Anna, B., Decesari, S., Gilardoni, S., Fischer, M., Fjaeraa, A. M., Fountoukis, C., George, C., Gomes, L., Halloran, P., Hamburger, T., Harrison, R. M., Herrmann, H., Hoffmann, T., Hoose, C., Hu, M., Hyvärinen, A., Hõrrak, U., Iinuma, Y., Iversen, T., Josipovic, M., Kanakidou, M., Kiendler-Scharr, A., Kirkevåg, A., Kiss, G., Klimont, Z., Kolmonen, P., Komppula, M., Kristjánsson, J.-E., Laakso, L., Laaksonen, A., Labonnote, L., Lanz, V. A., Lehtinen, K. E. J., Rizzo, L. V., Makkonen, R., Manninen, H. E., McMeeking, G., Merikanto, J., Minikin, A., Mirme, S., Morgan, W. T., Nemitz, E., O'Donnell, D., Panwar, T. S., Pawlowska, H., Petzold, A., Pienaar, J. J., Pio, C., Plass-Duelmer, C., Prévôt, A. S. H., Pryor, S., Reddington, C. L., Roberts, G., Rosenfeld, D., Schwarz, J., Seland, Ø., Sellegri, K., Shen, X. J., Shiraiwa, M., Siebert, H., Sierau, B., Simpson, D., Sun, J. Y., Topping, D., Tunved, P., Vaattovaara, P., Vakkari, V., Veefkind, J. P., Visschedijk, A., Vuollekoski, H., Vuolo, R., Wehner, B., Wildt, J., Woodward, S., Worsnop, D. R., van Zadelhoff, G.-J., Zardini, A. A., Zhang, K., van Zyl, P. G., Kerminen, V.-M., S Carslaw, K., and Pandis, S. N.: General overview: European Integrated project on Aerosol Cloud Climate and Air Quality interactions (EUCAARI) - integrating aerosol research from nano to global scales, Atmospheric Chemistry and Physics, 11, 13 061–13 143, https://doi.org/10.5194/acp-11-13061-2011, 2011.

Loubet, B., Cellier, P., Milford, C., and Sutton, M. A.: A coupled dispersion and exchange model for short-range dry deposition of atmospheric ammonia, Quarterly Journal of the Royal Meteorological Society, 132, 1733–1763, https://doi.org/10.1256/qj.05.73, 2006.

Meeder, J. and Nieuwstadt, F.: Large-eddy simulation of the turbulent dispersion of a reactive plume from a point source into a neutral atmospheric boundary layer, Atmospheric Environment, 34, 3563–3573, https://doi.org/10.1016/S1352-2310(00)00124-2, 2000.

Mensah, A. A., Holzinger, R., Otjes, R., Trimborn, A., Mentel, T. F., ten Brink, H., Henzing, B., and Kiendler-Scharr, A.: Aerosol chemical composition at Cabauw, The Netherlands as observed in two intensive periods in May 2008 and March 2009, Atmospheric Chemistry and Physics, 12, 4723–4742, https://doi.org/10.5194/acp-12-4723-2012, 2012.

Mylne, K. R. and Mason, P. J.: Concentration fluctuation measurements in a dispersing plume at a range of up to 1000 m, Quarterly Journal of the Royal Meteorological Society, 117, 177–206, https://doi.org/10.1002/qj.49711749709, 1991.

Nemitz, E., Sutton, M. A., Wyers, G. P., Otjes, R. P., Mennen, M. G., van Putten, E. M., and Gallagher, M. W.: Gas-particle interactions above a Dutch heathland: II. Concentrations and surface exchange fluxes of atmospheric particles, Atmospheric Chemistry and Physics, 4, 1007–1024, https://doi.org/10.5194/acp-4-1007-2004, 2004.

Nieuwstadt, F.: A large-eddy simulation of a line source in a convective atmospheric boundary layer—I. Dispersion characteristics, Atmospheric Environment. Part A. General Topics, 26, 485–495, https://doi.org/10.1016/0960-1686(92)90331-E, 1992.

Ouwersloot, H. G., Vilà-Guerau de Arellano, J., van Heerwaarden, C. C., Ganzeveld, L. N., Krol, M. C., and Lelieveld, J.: On the segregation of chemical species in a clear boundary layer over heterogeneous land surfaces, Atmospheric Chemistry and Physics, 11, 10 681–10 704, https://doi.org/10.5194/acp-11-10681-2011, 2011.

Ouwersloot, H. G., Moene, A. F., Attema, J. J., and Vilà-Guerau de Arellano, J.: Large-Eddy Simulation Comparison of Neutral Flow Over a Canopy: Sensitivities to Physical and Numerical Conditions, and Similarity to Other Representations, Boundary-Layer Meteorology, 162, 71–89, https://doi.org/10.1007/s10546-016-0182-5, 2017.

Pino, D., Jonker, H., Vilà-Guerau de Arellano, J., and Dosio, A.: Role of Shear and the Inversion Strength During Sunset Turbulence Over Land: Characteristic Length Scales, Boundary-Layer Meteorology, 121, 537–556, https://doi.org/10.1007/s10546-006-9080-6, 2006.

Rannik, ., Aubinet, M., Kurbanmuradov, O., Sabelfeld, K. K., Markkanen, T., and Vesala, T.: Footprint Analysis For Measurements Over A Heterogeneous Forest, Boundary-Layer Meteorology, 97, 137–166, https://doi.org/10.1023/A:1002702810929, 2000.

Ražnjević, A., van Heerwaarden, C., van Stratum, B., Hensen, A., Velzeboer, I., van den Bulk, P., and Krol, M.: Technical note: Interpretation of field observations of point-source methane plume using observation-driven large-eddy simulations, Atmospheric Chemistry and Physics Discussions, 2021, 1–29, https://doi.org/10.5194/acp-2021-614, 2021.

Remmelink, G., van Middelkoop, J., Ouweltjes, W., and Wemmenhove, H.: Handboek melkveehouderij 2020/21, no. 44 in Handboek / Wageningen Livestock Research, Wageningen Livestock Research, https://doi.org/10.18174/529557, over the year 2019/20, 2020.

RIVM: Landbouw, Emissiefactoren diercategorieën, Hoofdcategorie A: Rundvee, https://www.infomil.nl/onderwerpen/landbouw/emissiearme-stalsystemen/emissiefactoren-per/map-staltypen/hoofdcategorie/, accessed: 2021-01-28, 2021.

Sauter, F., van Zanten, M., van der Swaluw, E., Aben, J., de Leeuw, F., and van Jaarsveld, H.: The OPS-model: Description of OPS 4.5.2, Tech. rep., National Institute for Public Health and the Environment (RIVM, https://www.rivm.nl/media/ops/OPS-model.pdf, 2018.

Schaap, M., Timmermans, R. M. A., Roemer, M., Boersen, G. A. C., Builtjes, P. J. H., Sauter, F. J., Velders, G. J. M., and Beck, J. P.: The LOTOS–EUROS model: description, validation and latest developments, International Journal of Environment and Pollution, 32, 270 – 290, https://doi.org/10.1504/IJEP.2008.017106, 2008.

Schaug, J.: Quality assurance plane for EMEP, Tech. Rep. EMEP/CCC-Report 1/88, Norwegian Institute for Air Research, https://projects.nilu.no/ccc/reports/cccr1-88.pdf, 1988.

Schulte, R., van Zanten, M., Rutledge-Jonker, S., Swart, D., Wichink Kruit, R., Krol, M., van Pul, W., and Vilà-Guerau de Arellano, J.: Unraveling the diurnal atmospheric ammonia budget of a prototypical convective boundary layer, Atmospheric Environment, 249, 118 153, https://doi.org/10.1016/j.atmosenv.2020.118153, 2021.

Shah, A., Pitt, J. R., Ricketts, H., Leen, J. B., Williams, P. I., Kabbabe, K., Gallagher, M. W., and Allen, G.: Testing the near-field Gaussian plume inversion flux quantification technique using unmanned aerial vehicle sampling, Atmospheric Measurement Techniques, 13, 1467–1484, https://doi.org/10.5194/amt-13-1467-2020, 2020.

Shen, J., Chen, D., Bai, M., Sun, J., Coates, T., Lam, S. K., and Li, Y.: Ammonia deposition in the neighbourhood of an intensive cattle feedlot in Victoria, Australia, Sci Rep, 6, 2045–2322, https://doi.org/10.1038/srep32793, 2016.

Simpson, D., Benedictow, A., Berge, H., Bergström, R., Emberson, L. D., Fagerli, H., Flechard, C. R., Hayman, G. D., Gauss, M., Jonson, J. E., Jenkin, M. E., Nyíri, A., Richter, C., Semeena, V. S., Tsyro, S., Tuovinen, J.-P., Valdebenito, ., and Wind, P.: The EMEP MSC-W chemical transport model - technical description, Atmospheric Chemistry and Physics, 12, 7825 – 7865, https://doi.org/10.5194/acp-12-7825-2012, 2012.

Smit, L. A. M. and Heederik, D.: Impacts of Intensive Livestock Production on Human Health in Densely Populated Regions, GeoHealth, 1, 272–277, https://doi.org/10.1002/2017GH000103, 2017.

Sommer, S., Østergård, H., Løfstrøm, P., Andersen, H., and Jensen, L.: Validation of model calculation of ammonia deposition in the neighbourhood of a poultry farm using measured NH3 concentrations and N deposition, Atmospheric Environment, 43, 915–920, https://doi.org/10.1016/j.atmosenv.2008.10.045, 2009.

Stokstad, E.: Nitrogen crisis threatens Dutch environment- and economy, Science, 366, 1180–1181, https://doi.org/10.1126/science.366.6470.1180, 2019.

Stolk, A., Noordijk, H., and van Zanten, M.: Drogedepositiemetingen van ammoniak in Natura 2000-gebied Bargerveen, Tech. Rep. 680029001, National Institute for Public Health and the Environment (RIVM), Antonie van Leeuwenhoeklaan 9, 3721, MA Bilthoven, the Netherlands, https://rivm.openrepository.com/handle/10029/320523, 2014.

Sutton, M. A., Erisman, J. W., Dentener, F., and Möller, D.: Ammonia in the environment: From ancient times to the present, Environmental Pollution, 156, 583 – 604, https://doi.org/10.1016/j.envpol.2008.03.013, 2008.

Theobald, M. R., Løfstrøm, P., Walker, J., Andersen, H. V., Pedersen, P., Vallejo, A., and Sutton, M. A.: An intercomparison of models used to simulate the short-range atmospheric dispersion of agricultural ammonia emissions, Environmental Modelling & Software, 37, 90–102, https://doi.org/10.1016/j.envsoft.2012.03.005, 2012.

van Bruggen, C., Bannink, A., Groenestein, C., Huijsmans, J., Lagerwerf, L., Luesink, H., Ros, M., Velthof, G., Vonk, J., and van der Zee, T.: Emissies naar lucht uit de landbouw berekend met NEMA voor 1990-2019, no. 203 in WOt-technical report, Wettelijke Onderzoekstaken Natuur & Milieu, https://doi.org/10.18174/544296, project number WOT-04-008-031.01 and WOT-04-008-025.02, 2021.

van der Peet, G., Leenstra, F., Vermeij, I., Bondt, N., Puister, L., and van Os, J.: Feiten en cijfers over de Nederlandse veehouderijsectoren 2018, no. 1134 in Wageningen Livestock Research rapport, Wageningen Livestock Research, https://doi.org/10.18174/464128, 2018.

van der Swaluw, E., de Vries, W., Sauter, F., Aben, J., Velders, G., and van Pul, A.: High-resolution modelling of air pollution and deposition over the Netherlands with plume, grid and hybrid modelling, Atmospheric Environment, 155, 140–153, https://doi.org/10.1016/j.atmosenv.2017.02.009, 2017.

van Jaarsveld, J.: The Operational Priority Substances model: Description and validation of OPS-Pro 4.1, Tech. Rep. 500045001, National Institute for Public Health and the Environment (RIVM), Antonie van Leeuwenhoeklaan 9, 3721, MA Bilthoven, the Netherlands, https://www.rivm.nl/publicaties/operational-priority-substances-model, 2004.

Van Oss, R., Duyzer, J., and Wyers, P.: The influence of gas-to-particle conversion on measurements of ammonia exchange over forest, Atmospheric Environment, 32, 465–471, https://doi.org/10.1016/S1352-2310(97)00280-X, 1998.

van Zanten, M., Wichink Kruit, R., Hoogerbrugge, R., Van der Swaluw, E., and van Pul, W.: Trends in ammonia measurements in the Netherlands over the period 1993–2014, Atmospheric Environment, 148, 352–360, https://doi.org/10.1016/j.atmosenv.2016.11.007, 2017.

van Zanten, M. C., Sauter, F. J., Wichink Kruit, R. J., van Jaarsveld, J. A., and van Pul, W. A. J.: Description of the DEPAC module: Dry deposition modelling with DEPAC-GCN2010, Tech. Rep. 680180001, National Institute for Public Health and the Environment (RIVM), https://www.rivm.nl/bibliotheek/rapporten/680180001.pdf, 2010.

Verzijlbergh, R. A., Jonker, H. J. J., Heus, T., and Vilà-Guerau de Arellano, J.: Turbulent dispersion in cloud-topped boundary layers, Atmospheric Chemistry and Physics, 9, 1289–1302, https://doi.org/10.5194/acp-9-1289-2009, 2009.

Vesala, T., Kljun, N., Rannik, ., Rinne, J., Sogachev, A., Markkanen, T., Sabelfeld, K., Foken, T., and Leclerc, M.: Flux and concentration footprint modelling: State of the art, Environmental Pollution, 152, 653–666, https://doi.org/10.1016/j.envpol.2007.06.070, 2008.

Vilà-Guerau de Arellano, J., Talmon, A. M., and Builtjes, P.: A chemically reactive plume model for the NO-NO2-O3 system, Atmospheric Environment. Part A. General Topics, 24, 2237–2246, https://doi.org/10.1016/0960-1686(90)90255-L, 1990.

Vilà-Guerau de Arellano, J., Dosio, A., Vinuesa, J.-F., Holtslag, A. A. M., and Galmarini, S.: The dispersion of chemically reactive species in the atmospheric boundary layer, Meteorology and Atmospheric Physics, 87, 23–38, https://doi.org/10.1007/s00703-003-0059-2, 2004.

Vonk, J., Arets, E., Bannink, A., van Bruggen, C., Groenestein, C., Huijsmans, J., Lagerwerf, L., Luesink, H., Ros, M., Schelhaas, M., van der Zee, T., and Velthof, G.: Referentieraming van emissies naar de lucht uit landbouw en landgebruik tot 2030, met doorkijk naar 2035: Achtergronddocument bij de Klimaat- en Energieverkenning 2020, no. 1278 in Rapport / Wageningen Livestock Research, Wageningen Livestock Research, https://doi.org/10.18174/533503, 2020.

Vrieling, A. and Nieuwstadt, F.: Turbulent dispersion from nearby point sources—interference of the concentration statistics, Atmospheric Environment, 37, 4493–4506, https://doi.org/10.1016/S1352-2310(03)00576-4, 2003.

Wichink Kruit, R. and van Pul, W. A. J.: Ontwikkelingen in de stikstofdepositie, https://doi.org/10.21945/RIVM-2018-0117, 2018.

Wichink Kruit, R., Bleeker, A., Braam, M., van Goethem, T., Hoogerbrugge, R., Rutledge-Jonker, S., Stefess, G., Stolk, A., van der Swaluw, E., Voogt, M., and van Pul, A.: Op weg naar een optimale meetstrategie voor stikstof, https://doi.org/10.21945/RIVM-2021-0118, 2021.

Wichink Kruit, R. J., van Pul, W. A. J., Otjes, R. P., Hofschreuder, P., Jacobs, A. F. G., and Holtslag, A. A. M.: Ammonia fluxes and derived canopy compensation points over non-fertilized agricultural grassland in The Netherlands using the new GRadient Ammonia - High Accuracy - Monitoring (GRAHAM), Atmospheric Environment, 41, 1275 – 1287, https://doi.org/10.1016/j.atmosenv.2006.09.039, 2007.

Wichink Kruit, R. J., van Pul, W. A. J., Sauter, F. J., van den Broek, M., E., N., Sutton, M. A., Krol, M., and Holtslag, A. A. M.: Modeling the surface–atmosphere exchange of ammonia, Atmospheric Environment, 44, 945 – 957, https://doi.org/10.1016/j.atmosenv.2009.11.049, 2010.

WUR: Dutch Farm Accountancy Data Network, agriculture, https://www.agrimatie.nl/Binternet.aspx?ID=2&Bedrijfstype=2%403&SelectedJaren=2020&GroteKlassen=Alle+bedrijven, accessed: 2021-06-21, 2021.